THE UNIVERSITY of EDINBURGH

Edinburgh Research Explorer

Genomics of perivascular space burden unravels early mechanisms of cerebral small vessel disease

Citation for published version:
CHARGE Consortium, Duperron, M-G, Knol, MJ, Le Grand, Q, Evans, TE, Mishra, A, Tsuchida, A, Roshchupkin, G, Konuma, T, Trégouët, D-A, Romero, JR, Frenzel, S, Luciano, M, Hofer, E, Bourgey, M, Dueker, ND, Delgado, P, Hilal, S, Tankard, RM, Dubost, F, Shin, J, Saba, Y, Armstrong, NJ, Bordes, C, Bastin, ME, Beiser, A, Brodaty, H, Bülow, R, Carrera, C, Chen, C, Cheng, C-Y, Deary, IJ, Gampawar, PG, Himali, JJ, Jiang, J, Kawaguchi, T, Li, S, Macalli, M, Marquis, P, Morris, Z, Muñoz Maniega, S, Miyamoto, S, Okawa, M, Paradise, M, Parva, P, Rundek, T, Sargurupremraj, M, Schilling, S, Setoh, K, Soukarieh, O, Tabara, Y, Teumer, A, Thalamuthu, A, Trollor, JN, Valdés Hernández, MC, Vernooij, MW, Völker, U, Wittfeld, K, Wong, TY, Wright, MJ, Zhang, J, Zhao, W, Zhu, Y-C, Schmidt, H, Sachdev, PS, Wen, W, Yoshida, K, Joutel, A, Satizabal, CL, Sacco, RL, Bourque, G, Lathrop, M, Paus, T, Fernandez-Cadenas, I, Yang, Q, Mazoyer, B, Boutinaud, P, Okada, Y, Grabe, HJ, Mather, KA, Schmidt, R, Joliot, M, Ikram, MA, Matsuda, F, Tzourio, C, Wardlaw, JM, Seshadri, S, Adams, HHH & Debette, S 2023, 'Genomics of perivascular space burden unravels early mechanisms of cerebral small vessel disease', *Nature Medicine*, vol. 29, no. 4, pp. 950-962. https://doi.org/10.1038/s41591-023-02268-w

Digital Object Identifier (DOI):
10.1038/s41591-023-02268-w

Link:
Link to publication record in Edinburgh Research Explorer

Document Version:
Peer reviewed version

Published In:
Nature Medicine

General rights
Copyright for the publications made accessible via the Edinburgh Research Explorer is retained by the author(s) and / or other copyright owners and it is a condition of accessing these publications that users recognise and abide by the legal requirements associated with these rights.

Take down policy
The University of Edinburgh has made every reasonable effort to ensure that Edinburgh Research Explorer content complies with UK legislation. If you believe that the public display of this file breaches copyright please contact openaccess@ed.ac.uk providing details, and we will remove access to the work immediately and investigate your claim.

OPEN ACCESS

Download date: 10. Jun. 2023

Genomics of perivascular space burden unravels early mechanisms of cerebral small vessel disease

Marie-Gabrielle Duperron[1, 75], Maria J. Knol[2, 75], Quentin Le Grand[1, 75], Tavia E. Evans[3, 4, 75], Aniket Mishra[1, 75], Ami Tsuchida[5, 75], Gennady Roshchupkin[2, 4], Takahiro Konuma[6, 7], David-Alexandre Tregouët[1], Jose Rafael Romero[8, 9], Stefan Frenzel[10], Michelle Luciano[11], Edith Hofer[12, 13], Mathieu Bourgey[14, 15, 16], Nicole D. Dueker[17], Pilar Delgado[18], Saima Hilal[19, 20, 21], Rick M. Tankard[22, 23], Florian Dubost[4, 24], Jean Shin[25], Yasaman Saba[1, 26], Nicola J. Armstrong[23], Constance Bordes[1], Mark E. Bastin[27], Alexa Beiser[8,9,28], Henry Brodaty[22, 29], Robin Bülow[30], Caty Carrera[31], Christopher Chen[32, 33], Ching-Yu Cheng[34, 35], Ian J. Deary[11], Piyush G. Gampawar[26], Jayandra J. Himali[8, 9, 28, 36], Jiyang Jiang[22], Takahisa Kawaguchi[37], Shuo Li[8, 9], Melissa Macalli[1], Pascale Marquis[14, 15, 16], Zoe Morris[38], Susana Muñoz-Maniega[39], Susumu Miyamoto[40], Masakazu Okawa[41], Matthew Paradise[22], Parva Pedram[9, 42, 43], Tatjana Rundek[44, 45, 46], Murali Sargurupremraj[1], Sabrina Schilling[1], Kazuya Setoh[37, 47], Omar Soukarieh[1], Yasuharu Tabara[37, 47], Alexander Teumer[45], Anbupalam Thalamuthu[22], Julian N. Trollor[22, 48], Maria C. Valdés-Hernández[27, 49, 50], Meike W. Vernooij[2, 4], Uwe Völker[51], Katharina Wittfeld[10, 52], Tien Yin Wong[34], Margaret J. Wright[53, 54], Qiong Yang[9, 28], Junyi Zhang[55], Wanting Zhao[34, 56], Ycheng Zhu[55], Helena Schmidt[26], Perminder S. Sachdev[22, 57], Wei Wen[22], Kazumichi Yoshida[41], Anne Joutel[58], Claudia L. Satizabal[8, 9, 36], Ralph L. Sacco[44, 46, 59, 60, 61], Guillaume Bourque[14, 15, 16], the CHARGE consortium, Mark Lathrop[17], Tomas Paus[62, 63], Israel Fernandez-Cadenas[31, 64], Bernard Mazoyer[65, 66], Philippe Boutinaud[67], Yukinori Okada[6, 68, 69, 70], Hans J. Grabe[10, 52], Karen A. Mather[22, 71], Reinhold Schmidt[12], Marc Joliot[5], M. Arfan Ikram[2], Fumihiko Matsuda[37,76], Christophe Tzourio[1, 72, 76], Joanna M. Wardlaw[39, 76], Sudha Seshadri[8, 9, 36, 76], Hieab HH. Adams[3, 4, 73, 76]*, Stéphanie Debette[1, 74, 76]*

Affiliations

1. University of Bordeaux, Inserm, Bordeaux Population Health Research Center, team VINTAGE, UMR 1219, F-33000 Bordeaux, France
2. Department of Epidemiology, Erasmus MC University Medical Center, Rotterdam, The Netherlands
3. Department of Clinical Genetics, Erasmus MC University Medical Center, Rotterdam, The Netherlands
4. Department of Radiology and Nuclear Medicine, Erasmus MC Medical Center, Rotterdam, the Netherlands
5. Groupe d'Imagerie Neurofonctionelle, CEA, Univ. Bordeaux, CNRS, IMN, UMR 5293, F-33000 Bordeaux, France
6. Department of Statistical Genetics, Osaka University Graduate School of Medicine, 565-0871, Suita, Japan.
7. Central Pharmaceutical Research Institute, JAPAN TOBACCO INC, 569-1125, Takatsuki, Japan.
8. Department of Neurology, Boston University School of Medicine, Boston, MA, USA
9. The Framingham Heart Study, Framingham, MA, USA.
10. Department of Psychiatry and Psychotherapy, University Medicine Greifswald, Germany
11. Psychology, University of Edinburgh, UK
12. Clinical Division of Neurogeriatrics, Department of Neurology, Medical University of Graz, Austria
13. Institute for Medical Informatics, Statistics and Documentation, Medical University of Graz, Austria

14. Department of Human Genetics, McGill University, Montreal, QC Canada
15. McGill Genome Centre, Montreal, QC Canada
16. Canadian Centre for Computational Genomics, McGill University, Montreal, QC Canada
17. John P. Hussman Institute for Human Genomics, University of Miami, Miami, FL, USA
18. Institut de Recerca Vall d'hebron. Neurovascular Research Lab. Hospital Universitari Vall d'Hebron. Neurology Department. Universitat Autònoma de Barcelona. Barcelona, Spain.
19. Memory Aging and Cognition Center, National University Health System, Singapore
20. Department of Pharmacology, National University of Singapore, Singapore
21. Saw Swee Hock School of Public Health, National University of Singapore and National University Health System, Singapore
22. Centre for Healthy Brain Ageing, UNSW, Sydney, NSW 2052, Australia
23. Department of Mathematics and Statistics, Curtin University, Perth, WA 6102, Australia
24. Department of Medical Informatics, Erasmus MC University Medical Center, Rotterdam, The Netherlands
25. The Hospital for Sick Children, and Departments of Physiology and Nutritional Sciences, University of Toronto, Toronto, ON, Canada
26. Gottfried Schatz Research Center (for Cell Signaling, Metabolism and Aging), Medical University of Graz, Austria
27. Centre for Clinical Brain Sciences, University of Edinburgh & Edinburgh Imaging, University of Edinburgh, UK
28. Department of Biostatistics, Boston University School of Public Health, Boston, MA, USA
29. Dementia Collaborative Research Centre Assessment and Better Care, UNSW, Sydney, NSW 2031, Australia

30. Institute for Radiology and Neuroradiology, University Medicine Greifswald, Germany
31. Stroke Pharmacogenomics and Genetics group, Biomedical Research Institute Sant Pau (IIB Sant Pau), Barcelona Spain.
32. Memory Aging and Cognition Center, Department of Pharmacology, Yong Loo Lin School of Medicine, National University of Singapore, Singapore
33. Department of Psychological Medicine, Yong Loo Lin School of Medicine, National University of Singapore, Singapore
34. Singapore Eye Research Institute, Singapore National Eye Centre, Singapore
35. Duke-NUS Medical School, Singapore
36. Glenn Biggs Institute for Alzheimer's and Neurodegenerative Diseases and Department of Population Health Sciences, UT Health San Antonio, San Antonio, TX, USA
37. Center for Genomic Medicine, Kyoto University Graduate School of Medicine, Kyoto, Japan
38. Neuroradiology Department, Department Of Clinical Neurosciences, Western General Hospital, Edinburgh, UK
39. Division of Neuroimaging Sciences, Brain Research Imaging Centre, University of Edinburgh, UK
40. Kyoto University Hospital, Kyoto, Japan
41. Department of Neurosurgery, Kyoto University Graduate School of Medicine, Kyoto, Japan
42. Radiology Department, Boston University School of Medicine, Boston, MA, USA
43. Department of Radiology, Harvard Medical School, Boston, MA, USA
44. Department of Neurology, Miller School of Medicine, University of Miami, Miami, FL, USA

45. Institute for Community Medicine, University Medicine Greifswald, Germany
46. Evelyn F. McKnight Brain Institute, Department of Neurology, University of Miami, Miami, FL, USA
47. Graduate School of Public Health, Shizuoka Graduate University of Public Health, Shizuoka, Japan
48. Department of Developmental Disability Neuropsychiatry, UNSW, Sydney, NSW 2031, Australia
49. Row Fogo Centre for Research into Ageing and the Brain, University of Edinburgh, Edinburgh, UK
50. Western General Hospital, Crewe Rd, Edinburgh, EH4 2XU, UK
51. Interfaculty Institute for Genetics and Functional Genomics, University Medicine Greifswald, Germany
52. German Center for Neurodegenerative Diseases (DZNE), Site Rostock/Greifswald, Germany
53. Queensland Brain Institute, The University of Queensland, Brisbane 4072, Australia
54. Centre for Advanced Imaging, The University of Queensland, Brisbane 4072, Australia
55. Peking University Medical College Hospital, Beijing 107730, China
56. The Centre for Quantitative Medicine, Duke-NUS Medical School
57. Neuropsychiatric Institute, the Prince of Wales Hospital, Sydney, NSW 2031, Australia
58. Institut de Psychiatrie et Neurosciences de Paris, Université de Paris, Inserm U1266
59. Department of Public Health Sciences, Miller School of Medicine, University of Miami, Miami, FL, USA
60. Department of Human Genomics, Miller School of Medicine, University of Miami, Miami, FL, USA

61. Department of Neurosurgery, Miller School of Medicine, University of Miami, Miami, FL, USA
62. University of Montreal, Department of Psychiatry and Centre Hospitalier Universitaire Sainte Justine, Montreal, Quebec, H3T 1C5, Canada
63. University of Toronto, Departments of Psychology and Psychiatry, Toronto, Ontaior, Canada
64. Stroke Pharmacogenomics and Genetics group, Fundació per la Docència i la Recerca Mutua Terrassa, Terrassa, Spain.
65. University of Bordeaux, Institue for Neurodegenerative Disorders, UMR5293, F-33076 Bordeaux, France
66. Bordeaux University Hospital, F-33076 Bordeaux, France
67. Fealinx, Lyon, France
68. Laboratory of Statistical Immunology, Immunology Frontier Research Center (WPI-IFReC), Osaka University, 565-0871, Suita, Japan.
69. Integrated Frontier Research for Medical Science Division, Institute for Open and Transdisciplinary Research Initiatives, Osaka University, 565-0871, Suita, Japan.
70. Center for Infectious Disease Education and Research (CiDER), Osaka University, Suita 565-0871, Japan.
71. Neuroscience Research Australia, Sydney, NSW 2031, Australia
72. Bordeaux University Hospital, Department of Medical Informatics, F-33000 Bordeaux, France
73. Latin American Brain Health (BrainLat), Universidad Adolfo Ibáñez, Santiago, Chile
74. Bordeaux University Hospital, Department of Neurology, Institute of Neurodegenerative Diseases, F-33000 Bordeaux, France

75. These authors contributed equally to this work

76. These authors jointly supervised this work

*** Corresponding authors:**

Stéphanie Debette, Bordeaux Population Health research center, Inserm U1219, and Department of Neurology, Bordeaux University Hospital; University of Bordeaux, 146 rue Léo Saignat, 33076 Bordeaux Cedex, France. Telephone number: +33 5 57 57 16 59; Fax number: +33 5 47 30 42 09; e-mail: stephanie.debette@u-bordeaux.fr

&

Hieab H. H. Adams, Department of Clinical Genetics; Department of Radiology and Nuclear Medicine; Erasmus MC University Medical Center; Wytemaweg 80, 3015 CE, Rotterdam, the Netherlands; Telephone number: +31 10 70 33559; Fax number: +31 10 70 43489; e-mail address: h.adams@erasmusmc.nl

Perivascular space burden (PVS) is an emerging, poorly understood, magnetic resonance imaging (MRI)-marker of cerebral small vessel disease (cSVD), a leading cause of stroke and dementia. Genome-wide association studies in up to 40,095 participants (21 population-based cohorts, 66.3±8.6 years, 96.9% European) revealed 24 genome-wide significant PVS-risk loci, mainly in the white matter (WM). These were associated with WM-PVS already in young adults (N=1,748; 22.1±2.3 years) and enriched in early-onset leukodystrophy genes and genes expressed in fetal brain endothelial cells, suggesting early-life mechanisms. 53% of WM-PVS-risk loci showed nominally significant associations (24% after multiple-testing correction) in a Japanese population-based cohort (N=2,862; 68.3±5.3 years). Mendelian randomization supported causal associations of high blood pressure (BP) with basal ganglia (BG) and hippocampal (HIP) PVS, and of BG-PVS and HIP-PVS with stroke, accounting for BP. Most PVS loci point to novel pathways (extracellular matrix, membrane transport, developmental processes) and transcriptome-wide association studies prioritize 11 genes.

Perivascular spaces (PVS) are physiological spaces surrounding small vessel walls as they run from the subarachnoid space through the brain parenchyma.[1-3] Dilation of PVS observed on brain MRI is thought to be a marker of perivascular space dysfunction and speculated from preclinical studies to reflect impairment of brain fluid and waste clearance.[2,4]

PVS increase in number with age and vascular risk factors, especially hypertension.[5] They are associated with white-matter hyperintensities (WMH) of presumed vascular origin, lacunes, and cerebral microbleeds (CMB),[2] all MRI-features of cSVD, a leading cause of stroke and dementia with no specific mechanistic treatment to date.[6,7] PVS are detected on brain MRI much earlier than WMH, lacunes, or CMB,[8] and are described as the earliest stage of cSVD lesions on neuropathology.[9] Their pathophysiology is poorly understood.[7,10]

In experimental models, PVS appear to be important conduits for substrate delivery, flushing interstitial fluid, clearing metabolic waste (e.g. beta-amyloid peptide), and brain fluid regulation, as part of the "glymphatic system".[4,8] These processes were described to increase during sleep.[2,4,8] Mounting evidence suggests a major role of PVS in cerebral injury. Several studies suggested associations of PVS burden (number of visible PVS on brain MRI) with stroke,[2,7,11] AD pathology, and cerebral amyloid angiopathy.[12-14] Post-stroke edema has been linked to post-stroke PVS enlargement,[15] and in amyotrophic lateral sclerosis PVS dilation was observed and perivascular fibroblast proteins associated with survival.[16]

PVS burden is highly heritable.[17] Identifying genetic risk variants for PVS could be a powerful tool to decipher underlying biological pathways. We conducted genome-wide association study (GWAS) meta-analyses and whole exome/genome sequencing studies of extensive PVS burden in up to 40,095 and 19,178 older community participants. Given differential associations with risk factors and neurological traits[2,5,11] and anatomical differences,[18] we ran analyses separately for WM-PVS, BG-PVS, and HIP-PVS. We followed up

identified risk loci in independent samples of young healthy adults and older Japanese community participants and examined shared genetic determinants with other vascular and neurological traits. Leveraging tissue and cell-specific gene expression databases and drug target libraries, we conducted extensive bioinformatics exploration of identified PVS risk loci.

RESULTS

Genetic discovery

Twenty-one population-based cohorts were included, of which 18 for GWAS and 8 for whole exome association studies (**Supplementary Table 1**). We tested associations of extensive PVS burden with ~8 million single nucleotide polymorphisms (SNPs, minor allele frequency [MAF] ≥1%) in GWAS meta-analyses gathering up to 40,095 participants (66.3±8.6 years, 51.7% women, 66.7% hypertensives, **Supplementary Table 1-3**). We dichotomized PVS burden based on cut-offs closest to the top quartile of PVS distribution to account for differences in PVS quantification methods, image acquisition, and participant characteristics (**Supplementary Methods**). In total, 9,607 of 39,822, 9,189 of 40,000, and 9,339 of 40,095 participants had extensive PVS burden in WM, BG, and HIP.

The GWAS meta-analysis comprised 17 cohorts from the CHARGE consortium (N≤11,511),[19] with PVS quantification primarily on visual rating scales, and UK Biobank (UKB, N≤28,655) with computational PVS quantification (**Table 1**, **Supplementary Methods**). Participants were of European (N=38,871), Hispanic (N=717), East-Asian (N=339), and African-American (N=168) ancestry. We identified 22 independent genome-wide significant risk loci for extensive PVS burden (WM-PVS: 19, BG-PVS: 2, HIP-PVS: 3 [2 shared with WM-PVS]) and

two additional risk loci for WM-PVS in Europeans only, leading to 24 independent signals (**Table 1, Fig. 1, Supplementary Fig. 1-2**). There was no systematic inflation of association statistics (**Supplementary Table 4**, **Supplementary Fig. 1**).

We performed conditional logistic regression using GCTA-COJO (**Methods**) to seek independent association signals within genome-wide significant loci. Consistent with LD-clumping, this identified 2 independent signals at chr3p25.1 (*WNT7A*) and 6 at chr20q13.12 (*SLC13A3*, **Supplementary Fig. 2, Supplementary Table 5**), four of which with low frequency or rare variants (**Table 1**). The 6 polymorphisms at chr20q13.12 generated 8 haplotypes with haplotypic R^2>0.7 in the European-ancestry 3C-Dijon cohort (N=1,500, **Supplementary Results**). The two common rs2425881-A and rs2425884-C alleles, in very low LD with each other (r^2~0.05, D'~0.50), generated a common haplotype that was more frequent in individuals with extensive WM-PVS than those without (0.50 vs 0.47, OR=1.19 [95%CI:0.99-1.43]). The effect of this haplotype was amplified by 1.7 in the presence of the rs112407396-T allele (MAF=0.02), which has a high probability of being a regulatory variant (HaploReg, GTex, RegulomeDB). Next, to account for allelic heterogeneity between ancestries, we conducted cross-ancestry meta-analyses with MR-MEGA (**Methods**). There were no loci showing high heterogeneity in allelic effects across ancestries (PHet<0.01) and reaching genome-wide significance (**Supplementary Table 6**).

Using MAGMA and VEGAS we performed gene-based association analyses in European-ancestry participants, testing the combined association of variants within a gene with PVS, (**Methods**). MAGMA identified 28 gene-wide significant associations ($p<2.63x10^{-6}$), of which 12 in 8 loci not reaching genome-wide significance in the GWAS (WM-PVS: 3 [*INS-IGF2/IGF2, PRKAG2, LRP4/CKAP5*], BG-PVS: 4 [*SH3PXD2A, WNT3, ZMYND15*, *KCNRG/TRIM13/SPRYD7*], and HIP-PVS: 1 [*PDZRN4*], **Fig. 1, Supplementary Table 7**). VEGAS identified one additional

gene (*NSF*) for BG-PVS (same locus as *WNT3*, **Supplementary Table 7**). All were in suggestive GWAS loci ($p<5x10^{-6}$, **Supplementary Table 8**).

Using LD-score regression we estimated heritability at 11% for WM-PVS, 5% for BG-PVS, and 8% for HIP-PVS (**Supplementary Table 9**). We found moderate genetic correlation between BG-PVS and HIP-PVS (r_g(SE)=0.63(0.14), $p=7.23x10^{-6}$), and modest genetic correlation of WM-PVS with BG-PVS (r_g(SE)=0.24(0.12), p=0.055) and HIP-PVS (r_g(SE)=0.27(0.09), p=0.003). The genetic correlation between PVS in CHARGE and UKB was moderate to high for WM-PVS and HIP-PVS and weaker for BG-PVS (**Supplementary Table 10**). Associations with genome-wide significant PVS loci were highly consistent between the UKB and CHARGE contributions and between dichotomous and continuous PVS in UKB (**Supplementary Table 11-12)**. In sensitivity analyses in two representative cohorts (UKB and 3C-Dijon), continuous and dichotomous PVS measures were strongly correlated (Spearman-rho 0.61-0.80, **Supplementary Table 13)**.

To increase statistical power we conducted secondary multivariate association analyses using MTAG (**Methods**), including summary statistics from GWAS of other cSVD-markers (WMH-volume, lacunes, **Supplementary Methods**, **Supplementary Table 14**). We observed the highest gain in power for BG-PVS: 10 additional loci reached genome-wide significance, of which two also for HIP-PVS (*STN1, DEGS2/EVL*). Two MTAG BG-PVS loci (*CACNB2*, *NSF/WNT3*) and one MTAG WM-PVS locus (*VWA2*) were not described before with any MRI-marker of cSVD. Six loci showed greater significance in MTAG than with PVS, WMH-volume or lacunes alone: at *VWA2* (WM-PVS), *SH3PXD2A/STN1, COL4A2, CACNB2, NSF/WNT3* (BG-PVS) and *DEGS2/EVL* (BG-PVS, HIP-PVS).

Using whole exome sequencing (WES) and exome content of whole genome sequencing (WGS) data in 19,178 participants from UKB and the BRIDGET-consortium (**Methods,**

Supplementary Methods, Supplementary Table 1), of whom 4,531, 4,424, and 4,497 had extensive PVS in WM, BG, and HIP, we identified 19 variants in the chr1q25.3 locus associated with HIP-PVS, including two missense variants (rs20563 and rs20558) and one splice donor insertion (rs34133998) in *LAMC1* at $p<5x10^{-8}$, in strong LD with the GWAS sentinel variant (**Supplementary Table 15, Supplementary Results**).

Validation and expansion of findings across the lifespan and across ancestries

We explored associations of WM-PVS and BG-PVS risk variants with these phenotypes in young adults (i-Share study, N=1,748, 22.1±2.3 years) and in older Japanese community-dwelling persons (Nagahama study, N=2,862, 68.3±5.3 years, **Methods, Supplementary Methods**). We used a new AI-based method to derive quantitative WM-PVS and BG-PVS burden (HIP-PVS not available) and dichotomized it (top quartile vs. rest, **Supplementary Table 2, Supplementary Methods**). In total, 67% of WM-PVS loci reached nominally significant associations in at least one of the two follow-up cohorts ($p<0.05$ in i-Share and/or Nagahama), 43% of which at $p<1.09x10^{-3}$ (correcting for the number of loci tested), with consistent directionality of effect (a binomial test showed significant concordance of risk alleles, **Supplementary Table 12B)**. In i-Share, 52% of WM-PVS risk variants were associated with WM-PVS ($p<0.05$, of which 4 at $p<1.09x10^{-3}$, **Table 2, Supplementary Table 12A, Supplementary Fig. 3**). A WM-PVS rescaled weighted genetic risk score (wGRS) derived from European GWAS loci was associated with WM-PVS in i-Share (OR=1.17 [95%CI:1.09-1.25], $p=5.89x10^{-6}$ and beta(SE)=0.064(0.007), $p=2.06x10^{-19}$ for dichotomous and continuous measures). Although meta-regression suggested larger effect sizes at younger ages for lead variants at *OPA1* and *SLC13A3*, differences were not significant after removing the much younger i-Share cohort (**Supplementary Fig. 4**). In Nagahama, out of 17 available PVS risk loci

(6 were rare or monomorphic), 8 loci (53% of WM-PVS) were associated with continuous PVS burden at $p<0.05$, of which 4 at $p<1.09x10^{-3}$ and one at genome-wide significance (at *SLC13A3*, **Table 2, Supplementary Table 12A**). A European WM-PVS wGRS combining 14 independent loci (1000G JPT) was associated with WM-PVS in Nagahama (OR=1.18 [95%CI:1.13-1.24], $p=5.68x10^{-13}$ and beta(SE)=0.01(0.001), $p=7.18x10^{-18}$ for dichotomous and continuous measures). Although HIP PVS were not available in the follow-up cohorts, 2 of the 3 HIP PVS loci were shared with WM PVS and replicated with that phenotype.

Clinical correlates of identified PVS loci

We first examined whether PVS risk loci (lead and proxy variants with $r^2>0.9$) were associated with MRI-markers of brain aging, putative risk factors (vascular risk factors and sleep patterns), and common neurological diseases (stroke, AD, Parkinson disease), using the largest published GWAS (**Methods, Supplementary Methods**). Of 24 independent PVS risk loci, five (21%) were significantly ($p<3.3x10^{-5}$) associated with WMH volume and five (21%) with BP traits (in same and opposite directions, **Fig. 2**). Colocalization analyses suggested a shared causal variant for 2/3 of these associations (PP4>0.75, **Supplementary Table 16**). Sixteen PVS loci (67%) did not show any association with vascular or neurological traits, pointing to novel pathways (**Methods, Supplementary Table 17**).

Second, we explored genetic correlations of PVS burden with the same traits using LD-score regression (**Methods, Fig. 3, Supplementary Table 9**). We observed significant ($p<7.9x10^{-4}$) genetic correlation of BG-PVS with larger WMH and caudate nucleus volumes, and of HIP-PVS with larger hippocampal volume. BG-PVS and HIP-PVS showed significant genetic correlation with higher systolic blood pressure (SBP), diastolic blood pressure (DBP),

any stroke and ischemic stroke. Genetic correlations were consistent in secondary analyses conducted separately in CHARGE and UKB (**Supplementary Table 9**).

Third, we used two-sample Mendelian randomization to seek evidence for a causal association of putative risk factors with PVS burden and of PVS burden with neurological diseases, using generalised summary-data-based Mendelian randomization (GSMR), and confirming significant associations ($p<1.19x10^{-3}$) with RadialMR, Two-SampleMR and MR-CAUSE (**Methods**). Genetically determined higher SBP and DBP were consistently associated with BG-PVS, HIP-PVS and WM-PVS, although for WM-PVS the association with SBP was only nominally significant in RadialMR (**Supplementary Table 18, Supplementary Fig. 5**). There was no evidence for reverse causation using MR-Steiger, but some evidence of residual pleiotropy after removal of outlier variants for SBP and DBP (Radial-MR), with significant evidence for a causal model in MR-CAUSE for BG-PVS. Genetic liability to BG-PVS and HIP-PVS derived from a multitrait analysis accounting for other MRI-markers of cSVD (MTAG) was associated with an increased risk of any stroke, ischemic stroke, and small vessel stroke (SVS) for BG-PVS and SVS for HIP-PVS, suggesting that shared pathways between PVS, WMH, and lacunes may be causally associated with stroke (**Supplementary Methods, Supplementary Table 18**). In multivariable MR analyses accounting for SBP and DBP, genetic liability to BG-PVS and HIP-PVS was significantly associated with an increased risk of any stroke, ischemic stroke, and SVS (**Supplementary Table 19**).

Functional exploration of identified PVS loci

Using MAGMA and VEGAS2Pathway (**Methods**) we identified significant enrichment of PVS loci in pathways involved in extracellular matrix (ECM) structure and function, lymphatic

endothelial cell differentiation, cell motility, and thyroid hormone transport (**Supplementary Tables 20-21**).

Genes closest to PVS lead risk variants were significantly enriched in genes mutated in OMIM syndromes associated with leukodystrophy, leukoencephalopathy, or WMH (**Supplementary Table 22**), with a 20-fold enrichment in genes containing an intragenic lead variant (**Fig. 4**). This enrichment was 30-fold when focusing on WM-PVS loci only, comprising several genes involved in early-onset leukodystrophies: *GFAP* (chr17q21.31), mutations of which cause Alexander disease, a rare neurodegenerative disorder of astrocytes leading to psychomotor regression and death; *SLC13A3* (chr20q13.12), causing acute reversible leukoencephalopathy with increased urinary alpha-ketoglutarate; and *PNPT1* (chr2p16.1), causing Aicardi-Goutières syndrome and cystic leukoencephalopathy (**Fig. 4, Supplementary Results**). Although several genes near PVS lead risk variants were described to be involved in glioma we found no significant enrichment for glioma genes (**Supplementary Results**).

To seek evidence for a causal implication of specific genes and variants, we performed transcriptome-wide association studies (TWAS) using TWAS-Fusion (**Methods**), with European PVS GWAS summary statistics and the GTEXV7 multi-tissue (RNA-seq) database, focusing on brain, vascular and blood tissues. We found 36 transcriptome-wide significant expression-trait associations for WM-PVS, 25 for BG-PVS, and 7 for HIP-PVS that were significant in colocalization analyses (TWAS-COLOC), providing evidence of a shared causal variant between the corresponding gene expression and PVS (**Supplementary Table 23**). Most genes with significant expression-trait associations (12) were in genome-wide significant PVS risk loci, while 9 were outside GWAS loci requiring confirmation (**Fig. 5, Supplementary Results**). TWAS-COLOC signals were mostly observed in brain tissues (17 genes), but also vascular tissues (10 genes) and blood (2 genes).

To identify enrichment in specific brain cell types, we used a recently developed pipeline combining three cell-type enrichment methods, stratified LDscore, MAGMA, and H-MAGMA (**Supplementary Methods, Supplementary Table 24**). We observed significant enrichment in brain vascular endothelial cells for all PVS locations, based on a human single cell atlas of fetal gene expression (**Supplementary Methods**), and in pericytes and astrocytes for WM-PVS (**Supplementary Table 25**).

We explored brain expression pattern from development to adulthood of genes nearest to PVS loci, prioritizing TWAS-COLOC genes (**Methods**). Several genes showed important variations in expression levels throughout the lifecourse, some peaking in the pre-natal period (e.g. *LAMC1, UMPS*), suggestive of developmental mechanisms (**Supplementary Fig. 6**).

Finally, we conducted an exploratory search for enrichment of PVS genes in targets of drugs validated in other indications (**Methods**). We found significant enrichment of BG-PVS genes in targets for antiinfectives, driven by *CRHR1* (chr17q21.31, target for telavancin), and for diseases of the nervous system, driven by *MAPT* (chr17q21.31, target for davunetide); of HIP-PVS genes in targets for ear disease drugs, driven by *SERPIND1* (chr22q11.21, target for sulodexide, used for venous thrombosis prevention, **Supplementary Fig. 7**). We also observed significant enrichment of TWAS-significant HIP-PVS genes in vascular disease drugs, including simvastatin, vincamine, and macitentan (**Supplementary Fig. 8**).

DISCUSSION

In up to 40,095 participants from older population-based cohorts we identified 24 genome-wide significant risk loci for extensive PVS burden, predominantly for WM-PVS, and 6

additional loci after accounting for other MRI-markers of cSVD. In aggregate, identified WM-PVS risk loci were strongly associated with WM-PVS in 1,748 young healthy adults in their twenties and 2,862 older Japanese community-dwelling participants. Individually, more than half of WM-PVS loci were associated ($p<0.05$) with WM-PVS in each of these two smaller follow-up cohorts, and 67% in either of them (24% after multiple testing correction). While a third of PVS risk loci were shared with BP or WMH, two thirds reveal novel biological pathways, involving the ECM, membrane transport, and developmental processes, with a significant enrichment in genes expressed in fetal brain vascular endothelial cells and genes involved in early onset leukodystrophies. Using Mendelian randomization, genetically determined high SBP and DBP was associated with BG-PVS and HIP-PVS, and genetic liability to BG-PVS and HIP-PVS accounting for BP with increased risk of stroke, supporting causality. Using TWAS/colocalization and WES/WGS we provide evidence for causal implication of several genes warranting experimental follow-up. We show enrichment of PVS genes in targets for approved drugs for vascular, cognitive, and infectious diseases.

In line with the hypothesis that PVS is a marker of cSVD, moderate to high genetic correlation was observed with other MRI-markers of cSVD, primarily for BG- and HIP-PVS. Pathway analyses highlight ECM structure and function, known to play an important role in cSVD,[6,20,21] and several loci include genes involved in the matrisome (ECM and associated proteins), perturbations of which were proposed as a convergent pathologic pathway in cSVD (*LAMC1, EFEMP1, COL4A2, SH3PXD2A, VWA2*).[6,21] Several PVS risk loci (at *FOXF2*, *EFEMP1*, *KCNK2*, and *NBEAL1-ICA1L*) are known risk loci for other cSVD features (WMH, SVS),[6,22,23] and mutations in two MTAG genes cause monogenic SVD (at *COL4A1-COL4A2* and *STN1*).[24,25]

412 Consistent with distinct risk factor profiles,[2,11] the genetic architecture of PVS differed
413 across PVS locations, with WM-PVS showing the highest heritability and low genetic
414 correlation with BG-PVS and HIP-PVS.[1,2,17]

415 PVS have been described early in life,[8,26] but their clinical significance at young ages is
416 unknown. Our observation that genetic determinants of PVS discovered in older populations
417 are already associated with WM-PVS at age twenty suggests shared molecular mechanisms
418 underlying PVS in young and older age. This corroborates recently described associations of
419 WMH risk variants with changes in MRI-detected white matter microstructure at age twenty.[6]
420 The significant enrichment of PVS risk loci in genes involved in early-onset leukodystrophies
421 and expressed in fetal brain vascular endothelial cells supports involvement of developmental
422 processes. In spontaneously hypertensive stroke prone rats, closely modeling cSVD, intrinsic
423 endothelial cell dysfunction was observed at birth, including reduced tight junctions, as well
424 as altered oligodendrocyte maturation and myelination.[27] At the most significant WM-PVS
425 locus in young adults, *OPA1* harbors mutations causing autosomal dominant optical atrophy,
426 sometimes associated with multiple-sclerosis like illness, parkinsonism and dementia,[28] and
427 endothelial *OPA1* plays an important role in developmental angiogenesis.[29] These
428 observations corroborate epidemiological associations of early-life factors with cSVD-severity
429 in older age.[30]

430 The present effort has the largest East-Asian contribution compared with other large GWAS
431 of MRI-defined phenotypes,[31,32] with over half of available WM-PVS loci reaching nominally
432 significant, directionally consistent, associations in the Japanese follow-up study. The
433 prevalence of cSVD is higher in East-Asian than European populations.[33] Our results are an
434 important first step to establish the generalizability of cSVD genetic associations across

ancestries. Efforts to further enhance the non-European contribution to MRI-cSVD genomic studies, including in African-ancestry populations in whom cSVD is also more frequent, are of paramount importance.

The combination of PVS GWAS findings with TWAS and WES/WGS strongly supports putative causal genes, pointing to brain developmental processes, blood brain barrier (BBB) function, and response to brain damage.

WM-PVS associates with lower *LPAR1* expression in vascular tissues. *LPAR1* (chr9q31.3), expressed in oligodendrocytes, encodes a receptor for lysophosphatidic acid, an extracellular signaling small lipid and is involved in post-natal myelination and functional connectivity across brain regions.[35] An LPAR1 antagonist was found to attenuate brain damage after transient arterial occlusion, by decreasing inflammation,[36] and LPAR1 modulation may also impact neural regeneration.[37] Several drugs targeting LPAR1 are available (e.g. antidepressant mirtazapine[38]) or in development.[39] *WNT7A* (chr3p25.1) encodes a secreted signaling protein that targets the vascular endothelium,[40] and was implicated in brain angiogenesis and BBB regulation.[40] Loss of Wnt7a/b function in mice results in severe white matter damage.[41]

WM-PVS was associated with lower *ITGB5* (chr3q21.2) expression in whole blood. *ITGB5* encodes a beta subunit of integrin, and plays a central role in monogenic SVD.[42] Higher ITGB5 plasma levels were associated with decreased odds of cognitive impairment or dementia, lower brain amyloid burden and slower brain atrophy rates.[43] HIP-PVS was associated with lower expression of *LAMC1* (chr1q25.3, encoding Laminin gamma-1) in brain and higher expression in vascular tissues, while WES/WGS identified a splice donor variant at *LAMC1*. Laminins are ECM glycoproteins, and the major noncollagenous constituent of basement membranes. Genes encoding other basement membrane proteins (*NID2, COL4A1/2*) are implicated in cSVD.[6,22] Laminin regulates blood vessel diameter,[44] BBB integrity and function,[45]

and astrocytic laminin loss decreases expression of tight junction proteins and aquaporin-4 (AQP4),[45] a key modulator of glymphatic flow in experimental models.[8]

Some genes point to complex pleiotropic mechanisms. At chr2q33.2, also associated with WMH, SVS, AD, and caudate volume,[6,23,46,47] BG-PVS was associated with higher expression of *ICA1L* in brain tissues and of *NBEAL1* in vascular tissues, similar to TWAS of WMH and SVS.[6,22] *ICA1L* (encoding islet cell autoantigen-1 like and predominantly expressed in endothelial cells) harbors mutations causing juvenile amyotrophic lateral sclerosis,[48] while *NBEAL1* (encoding neurobeachin-like 1 protein) modulates LDL-receptor expression.[49]

Our study points to an important involvement of solute carriers (SLCs), the largest family of transporters and candidates for drug target development,[50] in PVS pathophysiology. *SCL13A3* encodes a plasma membrane Na+/dicarboxylate cotransporter expressed in kidney, astrocytes, and choroid plexus.[51] Mutations in *SLC13A3* cause acute reversible leukoencephalopathy with increased urinary alpha-ketoglutarate,[51] where SLC13A3 loss-of-function may affect elimination of organic anions and xenobiotics from the cerebrospinal fluid (CSF).[51] Mutations in *SLC2A10* cause arterial tortuosity syndrome,[52] arterial tortuosity being described to be associated with PVS burden and cSVD.[32] WM-PVS was associated with lower *SLC20A2* expression in brain tissue (**Fig. 5**). *SLC20A2,* involved in phosphate transport, harbors loss-of-function mutations causing idiopathic familial basal ganglia calcification, a neurodegenerative disorder with inorganic phosphate accumulation in the ECM.[53] Suggestive associations with PVS ($p<5x10^{-6}$) and recently reported SVS loci also involve SLC genes (**Supplementary Table 8**).[22] Given their role in CSF secretion and substance transport at the blood-CSF barrier,[54] SLCs could be involved in interstitial fluid accumulation adjacent to the PVS.[55]

Consistent with other SVD phenotypes we observed evidence for a causal association of BP with PVS. Experimental work suggests that the perivascular pump becomes less efficient with increasing BP, reducing net forward flow in the PVS. These effects were found to be larger at more distal locations, where arteries have thinner and less muscular walls.[56] Such hemodynamic and anatomic differences[1] could, perhaps, at least partly explain the more significant association of BP with BG-PVS and HIP-PVS compared to WM-PVS. In contrast, WM-PVS were associated with cerebral amyloid angiopathy (CAA)[12] and with higher brain amyloid deposition on positron emission tomography, across the clinical spectrum of CAA.[13] The updated Boston Criteria (V2.0) for CAA include severe WM-PVS as a novel diagnostic criterion.[14]

The significant genetic correlation of BG-PVS and HIP-PVS with any stroke and ischemic stroke and robust evidence for a possible causal association of BG-PVS and HIP-PVS with any stroke, ischemic stroke, and SVS, accounting for BP, strongly support the clinical relevance of PVS. We also found nominally significant evidence for genetic correlation and possible causal relation of BG-PVS and HIP-PVS with (deep) ICH (**Supplementary Table 9 & 18**), consistent with epidemiological findings.[11] Considering the association of HIP-PVS with lower *LAMC1* expression in brain, it is striking to note that conditional knock-out of laminin in astrocytes leads to deep ICH in mice.[57] This is reminiscent of known associations of variants in *COL4A1/A2*, encoding another basement membrane protein, with monogenic and multifactorial deep ICH.[46,58] Significant enrichment of PVS genes in targets of drugs validated or under investigation for vascular and cognitive disorders highlights the potential of PVS genetics for cSVD drug discovery.

This is the first study exploring the genetic determinants of PVS, using a comprehensive gene-mapping strategy and extensive bioinformatics follow-up. To account for heterogeneity in PVS quantification methods we pragmatically dichotomized PVS variables based on the top quartile of the distribution, which may be less powerful than continuous measures. This may have been most prominent for BG-PVS, for which the genetic correlation pattern between CHARGE and UKB was low, in contrast with WM-PVS and HIP-PVS. Reassuringly, loci identified using dichotomous PVS phenotypes were also associated with continuous PVS burden in studies where computational methods were available (UKB, i-Share, Nagahama), mostly with more significant p-values. A conservative approach will also have helped minimize the effect of accidentally including WMH in the PVS measures, a problem which some computational PVS methods have not yet overcome. Strikingly, 67% of WM-PVS loci were associated at least nominally with WM-PVS in one or both follow-up cohorts, despite considerably smaller samples and distinct age and ancestry, with consistent directionality. This suggests that our genomic discovery approach, although likely conservative, led to robust findings. With increasing development of AI-based computational methods for PVS quantification, future genomic studies will likely have even greater power to detect genetic associations, to enable studying the genomics of total PVS volume, accounting for differences in individual PVS volume, width, length, shape,[59] density, location, anatomical predominance and to run sex-specific analyses.

In conclusion, in this first gene-mapping study of PVS, one of the earliest MRI-markers of cSVD, we describe 24 genome-wide significant risk loci, with 6 additional loci in secondary multivariate analyses accounting for other cSVD markers. Our findings provide completely novel insight into the biology of PVS across the adult lifespan and its contribution to cSVD

pathophysiology, with potential for genetically informed prioritization of drug targets for prevention trials of cSVD, a major cause of stroke and dementia worldwide.

REFERENCES (60 main text references will be pasted here before submission – see full list at the end)

Figure 1: Illustration of extensive perivascular space burden and Manhattan plot of the PVS GWAS meta-analysis

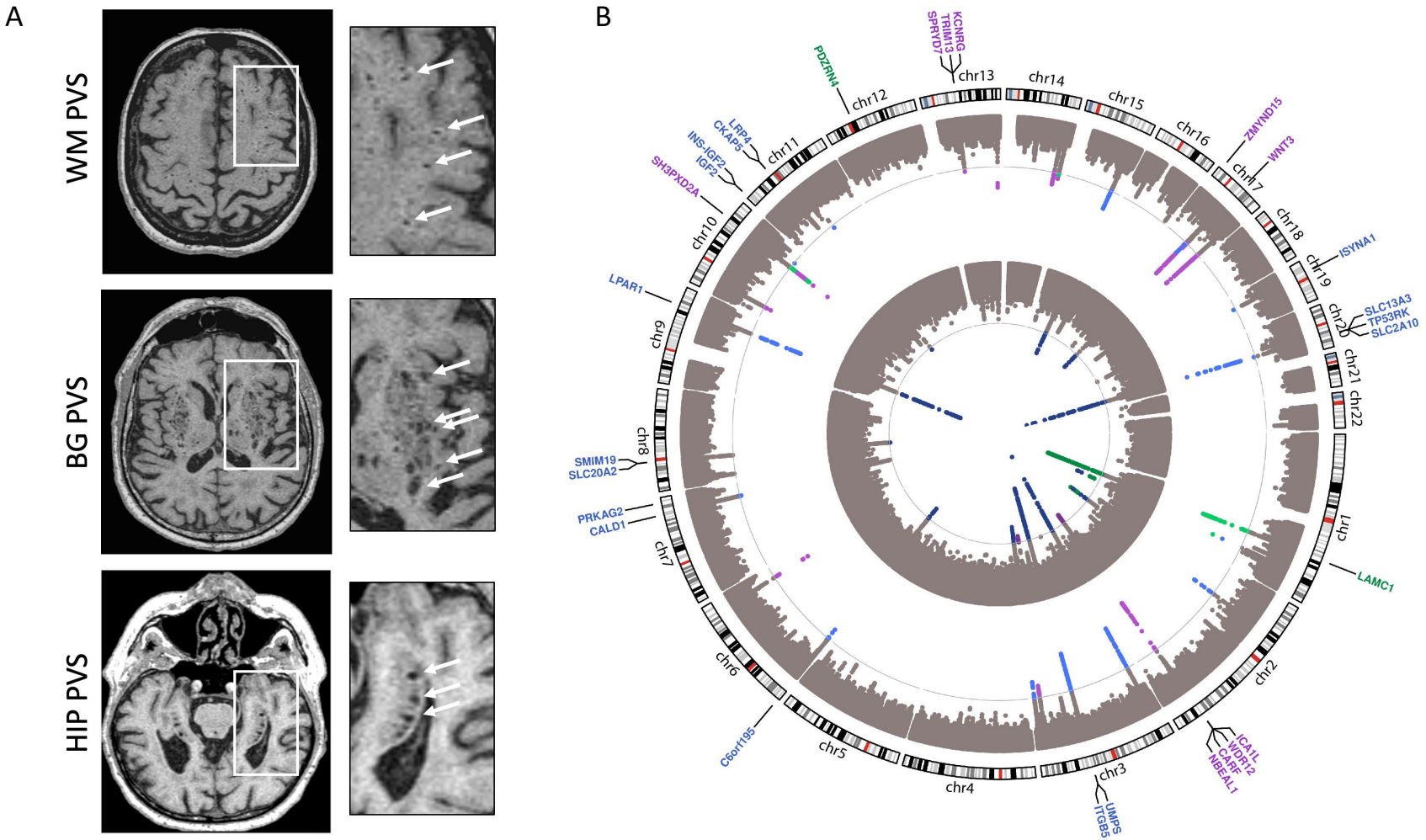

A. T1-weighted axial brain magnetic resonance images. Extensive perivascular space burden in basal ganglia (circles, top, BG PVS), white matter (arrows, middle, WM PVS), and hippocampus (arrows, bottom, HIP PVS) on T1-weighted axial magnetic resonance images; B. The inner circle corresponds to the GWAS results (combined meta-analyses), the middle circle to MTAG results, and the outer circle to gene-based test results. Results for WM PVS are in blue, for BG PVS in purple and for HIP PVS in green. The grey line corresponds to the genome-wide significance threshold ($p=5x10^{-8}$).

Figure 2: Association of PVS loci with vascular risk factors and other MRI-markers of SVD

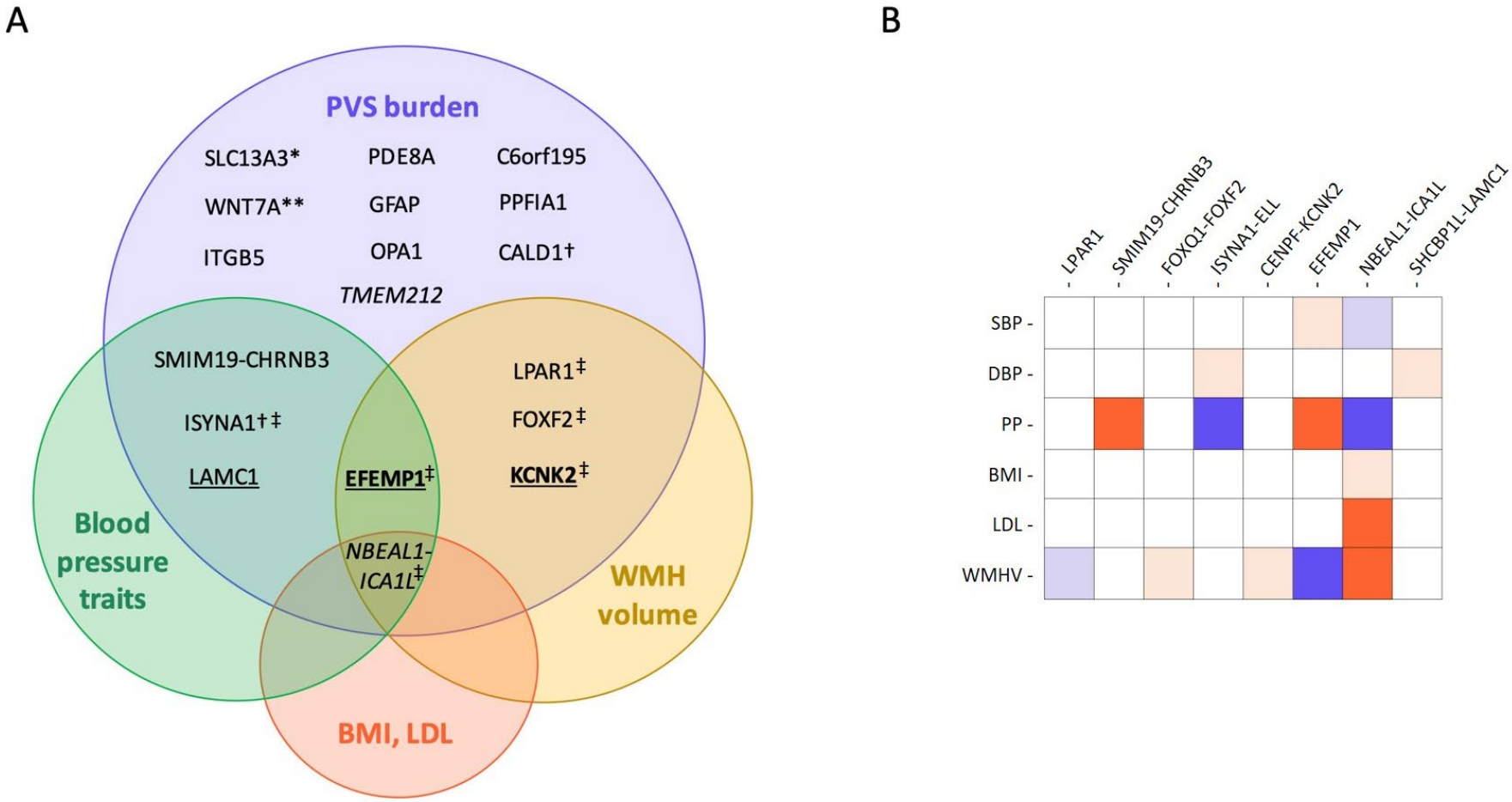

A. Venn diagram displaying significant association of genome-wide significant (GWS) risk loci for PVS with vascular risk factors and other MRI-markers of cSVD: in italic for BG PVS; underligned for HIP PVS (bold if also WGS for WM PVS); all others for WM PVS ($p<7.9x10^{-4}$); * 6

independent loci; ** 2 independent loci; † genome-wide significant in Europeans only; ‡ in colocalization analyses the posterior probability PP4 was higher than 75% for these loci (only with WMH at *NBEAL1-ICA1L*). B. Direction of association and level of significance of pleiotropic SNPs displayed in A: in red when the risk allele for extensive PVS burden is positively associated with the trait, in blue when the PVS risk allele is negatively associated with the trait (unexpected direction), in dark color for genome-wide significant associations, and in light color for significant association after multiple testing correction ($p<7.9x10^{-4}$); PVS, perivascular spaces; SBP, systolic blood pressure; DBP, diastolic blood pressure; PP, pulse pressure; BMI, body mass index; LDL, LDL-cholesterol; WMH(V): white matter hyperintensity (volume).

Figure 3: Genetic correlations of extensive PVS burden with risk factors, neurological diseases, and other MRI-markers of brain aging

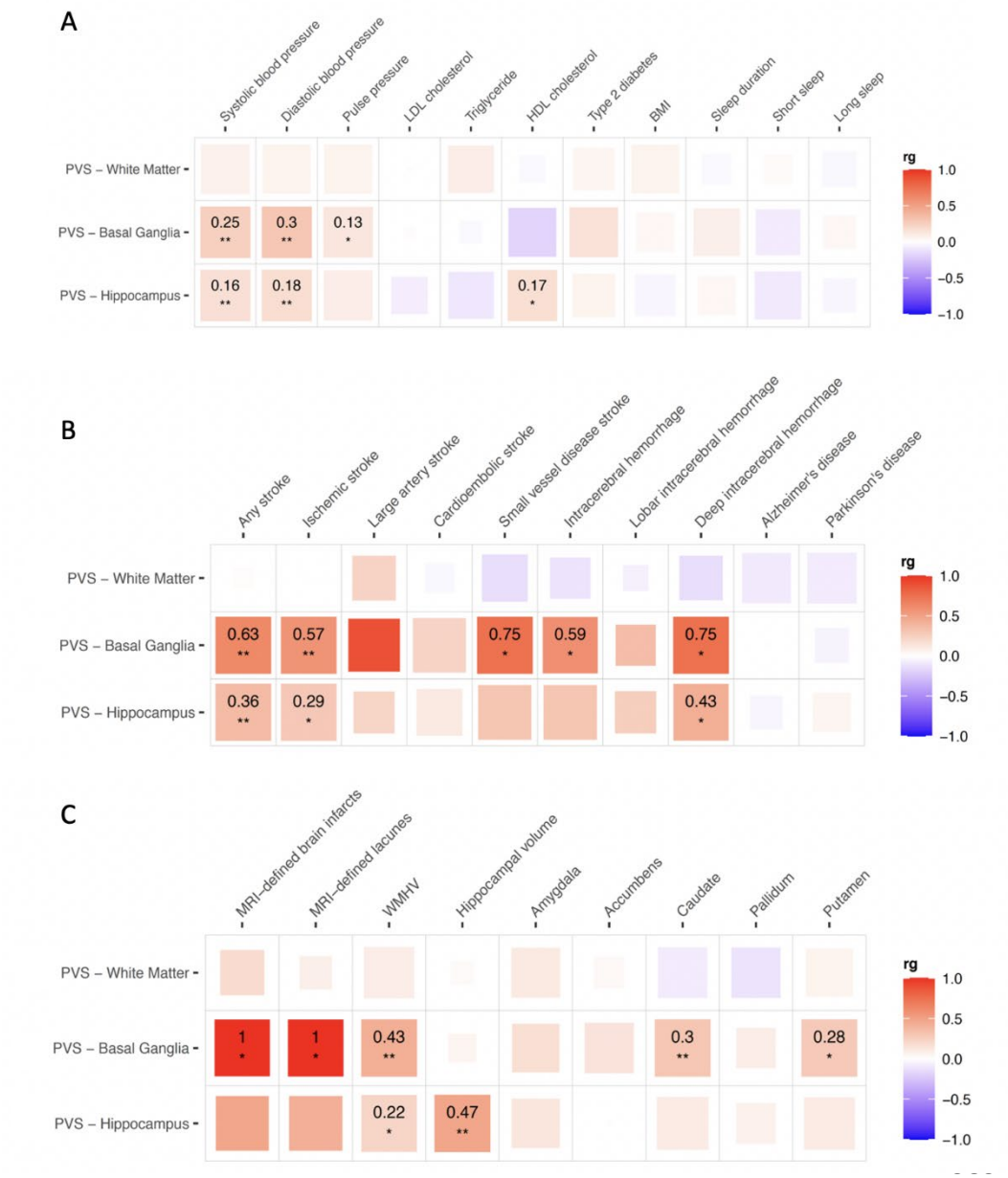

Genetic correlation using LDscore regression of extensive PVS burden with (A) putative risk factors, (B) neurological diseases, and (C) other MRI-markers of brain aging; LDSR: LD score regression; GSMR: Generalized Summary-data-based Mendelian Randomization; *p<0.05; **$p<7.9x10^{-4}$ correcting for 21 independent phenotypes and the three PVS locations. Larger colored squares correspond to more significant p-values and the colors represent the direction of the genetic correlation (positive in red, negative in blue).

592 **Figure 4. Enrichment of PVS risk loci in genes mutated in OMIM syndromes**

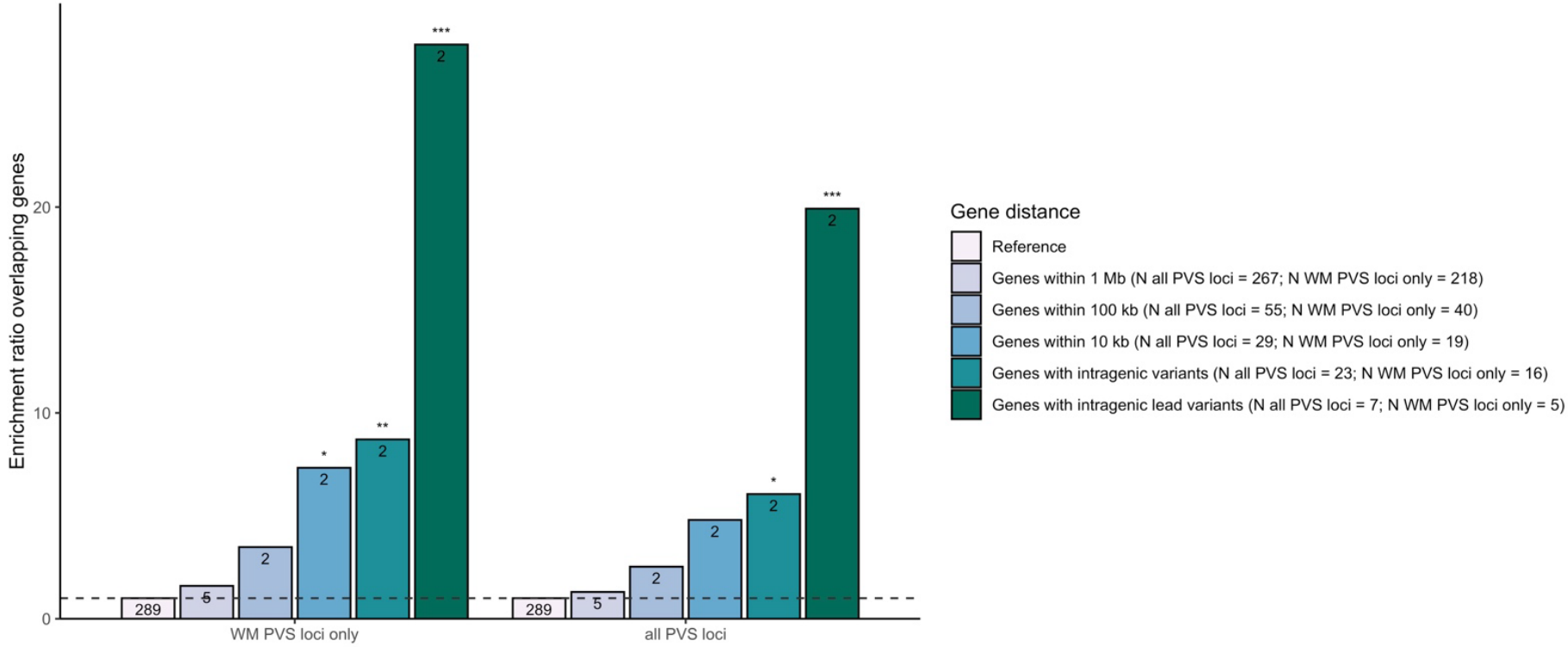

593

594 Enrichment of all PVS loci (left) and WM PVS loci only (right) in genes mutated in OMIM syndromes associated with WMH, leukodystrophy,

595 leukoencephalopathy, stroke or dementia, according to distance from the lead variant; * p<0.05 ; ** p<(0.05/5); *** p<(0.05/5/2)

596

Figure 5. Transcriptome-wide significant genes with extensive PVS burden

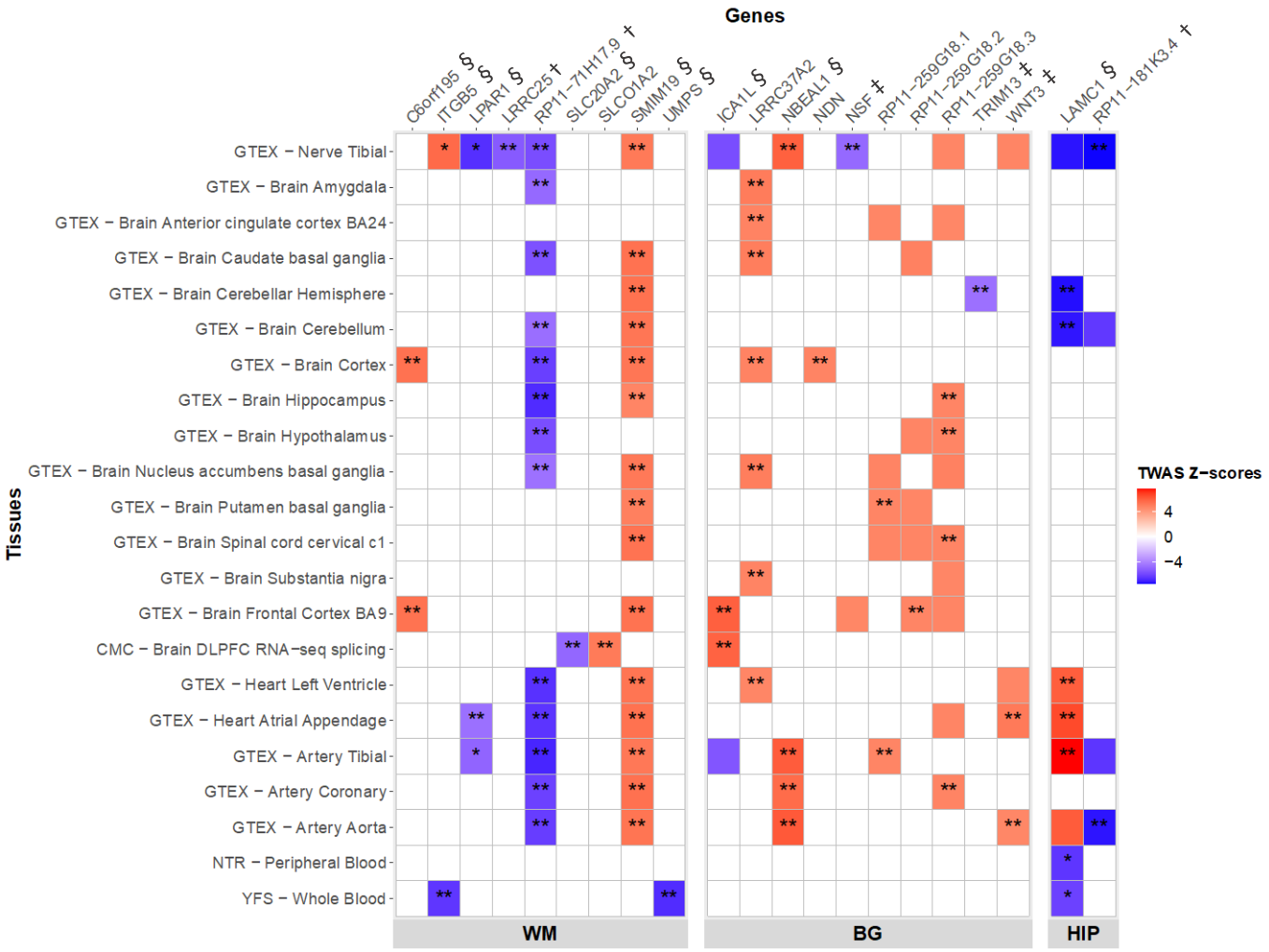

* significant result in the TWAS and conditional analyses; ** significant result in the TWAS and conditional analyses, and with a COLOC PP4 > 0.75; genes in loci identified in the GWAS (†) or gene-based test (‡) or in both GWAS and gene-based test (§)

603 **Table 1. Genetic variants associated with high perivascular spaces burden**

604

Region	SNP ALL	chr:position	EA/OA	EAF	Function	Nearest gene(s)	Effect (beta)‡	SE‡	Z-score§	Dir§	N ext-PVS / total	p-val EUR	p-val All	Het p-val
PVS in white matter														
20q13.12	rs6011998	20:45269867	C/T	0.95	intronic	*SLC13A3*	0.087	0.009	10.65	++++	9502/39128	**1.90E-24**	**1.80E-26**	0.11
3p25.1	rs13079464	3:13822439	C/G	0.46	intergenic	*WNT7A*	0.026	0.004	8.70	++++	9614/39822	**8.64E-17**	**3.41E-18**	0.59
20q13.12	rs2425884	20:45258292	C/T	0.57	intronic	*SLC13A3*	0.029	0.004	8.63	+-+-	9614/39822	**2.60E-18**	**6.02E-18**	0.14
9q31.3	rs10817108*	9:113658671	A/G	0.21	intronic	*LPAR1*	0.029	0.004	8.20	+++?	9550/39516	**1.07E-15**	**2.46E-16**	0.75
20q13.12	rs2425881	20:45255618	A/G	0.83	intronic	*SLC13A3*	0.033	0.005	7.68	+-+?	9496/39087	**2.02E-15**	**1.59E-14**	0.06
3q21.2	rs3772833	3:124518362	G/A	0.83	intronic	*ITGB5, UMPS*	0.032	0.005	7.67	+++?	9496/39087	**2.15E-13**	**1.76E-14**	0.39
20q13.12	rs112407396	20:45276381	T/A	0.03	intronic	*SLC13A3*	0.078	0.012	6.91	+???	8426/34530	**4.81E-12**	**4.81E-12**	1.00
1q41	rs10494988	1:215141570	C/T	0.63	intergenic	*CENPF, KCNK2*	0.021	0.004	6.54	++++	9614/39822	**2.23E-10**	**6.03E-11**	0.69
20q13.12	rs72485816†	20:45314435	T/C	0.96	UTR3	*TP53RK, SLC13A3*	0.059	0.010	6.45	++?-	9114/37342	**1.47E-10**	**1.12E-10**	0.87
15q25.3	rs8041189	15:85686327	G/A	0.70	intergenic	*PDE8A*	0.022	0.004	6.44	+-??	9486/39315	**7.30E-11**	**1.24E-10**	0.31
3p25	rs4685022	3:13832611	G/A	0.65	intergenic	*WNT7A*	0.019	0.004	6.40	+++?	9576/39654	**2.36E-09**	**1.58E-10**	0.11
2p16.1	rs7596872	2:56128091	C/A	0.90	intronic	*EFEMP1*	0.033	0.006	6.31	+-??	9333/38442	**1.00E-10**	**2.80E-10**	0.11
17q21.31	rs1126642	17:42989063	C/T	0.96	exonic	*GFAP*	0.051	0.009	6.23	+?+?	9119/37466	**6.19E-10**	**4.67E-10**	0.72
3q29	rs687610†	3:193515781	G/C	0.43	intergenic	*OPA1*	0.021	0.004	6.20	+++-	9614/39822	**2.99E-10**	**5.81E-10**	0.76
6p25.2	rs4959689	6:2617122	C/A	0.58	intergenic	*C6orf195*	0.020	0.004	6.03	++++	9582/39695	**3.37E-09**	**1.63E-09**	1.00
20q13.12	rs56104388	20:45302135	T/C	0.99	intronic	*SLC13A3*	0.101	0.017	5.85	+???	7626/30916	**4.80E-09**	**4.80E-09**	1.00
11q13.3	rs12417836	11:70089700	T/C	0.07	intergenic	*FADD, PPFIA1*	0.034	0.007	5.58	+-+?	9464/38960	**1.56E-08**	**2.47E-08**	0.40
8p11.21	rs2923437†	8:42425399	A/C	0.41	intergenic	*SMIM19, CHRNB3, SLC20A2*	0.018	0.004	5.49	++--	9614/39822	**4.73E-08**	**4.08E-08**	0.14
6p25.3	rs1922930	6:1364691	C/A	0.12	intergenic	*FOXQ1, FOXF2*	0.029	0.006	5.47	++??	9406/38748	**3.60E-08**	**4.62E-08**	0.48
19p13.11	rs2385089	19:18550434	A/C	0.74	intergenic	*ISYNA1, ELL, LRRC25**	0.023	0.005	5.49	+++-	9614/39822	**4.14E-08**	5.73E-08	0.57
7q33	rs10954468	7:134434661	C/A	0.40	intergenic	*BPGM, CALD1**	0.019	0.004	5.52	+-?+	9524/39483	**3.39E-08**	8.79E-08	0.29
PVS in basal ganglia														
2q33.2	rs4675310†	2:203880834	A/G	0.87	intronic	*NBEAL1, ICA1L*	0.027	0.005	5.92	++??	9011/39243	**2.71E-09**	**3.27E-09**	0.64
3q26.31	rs6769442	3:171565463	G/A	0.75	intronic	*TMEM212*	0.020	0.004	5.74	++?+	9101/39788	**1.68E-08**	**9.34E-09**	0.96

PVS in hippocampus															
1q25.3	rs10797812†	1:182984597	A/G	0.54	intergenic	*SHCBP1L, LAMC1*	0.027	0.004	7.84	++++	9399/40095	**1.67E-14**	**4.39E-15**	0.68
2p16.1	rs78857879†	2:56135099	G/A	0.90	intronic	*EFEMP1*	0.038	0.006	6.43	+???	9033/38008	**8.20E-11**	**1.31E-10**	1.00
1q41	rs6540873	1:215137222	A/C	0.62	intergenic	*CENPF, KCNK2*	0.020	0.004	5.95	+--+	9399/40095	**1.38E-09**	**2.72E-09**	0.11

PVS indicates perivascular spaces; EA, effective allele; OA, other allele; EAF, effective allele frequency, N with ext-PVS correspond to the number of participants with extensive PVS burden in the combined meta-analysis; p-val all, p-value in the combined meta-analysis; Het p-value corresponds to the heterogeneity p-value in the meta-analysis (except for rs2385089 and rs10954468 for which the European combined meta-analysis het p-value is reported); N total corresponds to the number of participants in the combined meta-analysis; dir corresponds to the association direction of the EA with the phenotype (extensive PVS burden versus the rest) for European, Hispanic, Asian, and African American ancestry studies, in this order; genome-wide significant loci (p-value<$5x10^{-8}$) are in bold; Z-scores of the combined sample size weighted meta-analysis are represented, except for the 2 SNPs reaching genome-wide significance in Europeans only (rs2385089, rs10954468) for which the European meta-analysis Z-score is reported. *Genome-wide significant association in Europeans only; †for these loci, the lead SNP was different in the European meta-analysis: rs72485816→rs6094423; rs687610→rs6444747; rs2923437→ rs62509329; rs4675310→ rs140244541; rs10797812→ rs2022392; rs78857879→ rs7596872; pvalue of the top SNP of this locus in the European meta-analysis (r^2>0.10 with the top SNP of this locus in the European meta-analysis); ‡ from inverse-variance weighted meta-analysis; § from Z-score based meta-analysis

Table 2. Association of genome-wide significant WM and BG PVS risk loci with PVS burden across the lifespan (i-Share study, N=1,748) and across ancestries (Nagahama study, N=2,862)

GWAS meta-analysis				i-Share (dichotomous)		i-Share (continuous)		Nagahama (dichotomous)		Nagahama (continuous)	
SNP	**chr:position**	**EA/OA**	**Nearest gene(s)**	**OR [95%CI]**	**p**	**Beta (SE)**	**p**	**OR [95%CI]**	**p**	**Beta (SE)**	**P**
PVS in white matter											
rs6011998	20:45269867	C/T	*SLC13A3*	1.26 [0.83-1.92]	0.28	0.164 (0.04)	**4.20E-05†**	1.69 [1.33-2.13]	**1.22E-05†**	0.037 (0.008)	**6.21E-07†**
rs13079464	3:13822439	C/G	*WNT7A*	1.12 [0.91-1.40]	0.29	0.014 (0.02)	0.50	1.16 [0.97-1.40]	0.11	0.015 (0.006)	**1.50E-02**
rs2425884	20:45258292	C/T	*SLC13A3*	1.18 [0.95-1.45]	0.13	0.077 (0.02)	**2.98E-04†**	1.29 [1.09-1.52]	**3.48E-03**	0.026 (0.005)	**1.77E-06†**
rs10817108	9:113658671	A/G	*LPAR1*	0.90 [0.69-1.17]	0.44	0.058 (0.03)	**2.23E-02**	1.18 [0.98-1.43]	0.07	0.017 (0.006)	**4.10E-03**
rs2425881	20:45255618	A/G	*SLC13A3*	1.47 [1.03-2.01]	**1.40E-02**	0.063 (0.03)	**2.62E-02**	1.18 [1.01-1,37]	**3.66E-02**	0.014 (0.005)	**4.68E-03**
rs3772833	3:124518362	G/A	*ITGB5, UMPS*	1.22 [0.89-1.66]	0.21	0.006 (0.03)	0.85	1.06 [0.88-1.29]	0.51	0.008 (0.006)	0.16
rs112407396	20:45276381	T/A	*SLC13A3*	1.47 [0.77-2.78]	0.24	0.147 (0.07)	**3.13E-02**	NA	NA	NA	NA
rs10494988	1:215141570	C/T	*CENPF, KCNK2*	1.18 [0.95-1.47]	0.14	0.079 (0.02)	**1.94E-04†**	1.01 [0.86-1.18]	0.90	-0.002 (0.005)	0.67
rs72485816	20:45314435	T/C	*TP53RK, SLC13A3*	1.01 [0.56-1.80]	0.98	0.093 (0.06)	0.095	1.32 [1.10-1.59]	**2.83E-03**	0.033 (0.006)	**1.91E-08‡**
rs8041189	15:85686327	G/A	*PDE8A*	1.14 [0.89-1.44]	0.30	0.041 (0.02)	0.073	1.67 [0.84-3.33]	0.14	0.046 (0.021)	**2.40E-02**
rs4685022	3:13832611	G/A	*WNT7A*	1.12 [0.88-1.42]	0.34	0.023 (0.02)	0.31	1.15 [0.97-1.36]	0.10	0.010 (0.005)	0.075*
rs7596872	2:56128091	C/A	*EFEMP1*	1.65 [1.10-2.46]	**1.14E-02**	**0.089 (0.03)**	**1.10E-02**	NA	NA	NA	NA
rs1126642	17:42989063	C/T	*GFAP*	1.13 [0.65-1.97]	0.67	0.127 (0.05)	**1.27E-02**	1.35 [1.09-1.67]	0.11	0.033 (0.007)	**9.88E-07†**
rs687610	3:193515781	G/C	*OPA1*	1.46 [1.18-1.80]	**4.88E-04†**	**0.109 (0.02)**	**1.29E-07†**	0.95 [0.81-1.13]	0.59	0.006 (0.005)	0.28
rs4959689	6:2617122	C/A	*C6orf195*	1.10 [0.89-1.37]	0.37	0.022 (0.02)	0.30	NA	NA	0.024 (0.026)	0.34*
rs56104388	20:45302135	T/C	*SLC13A3*	1.30 [0.40-4.24]	0.67	0.274 (0.11)	**1.47E-02**	NA	NA	NA	NA
rs12417836	11:70089700	T/C	*FADD, PPFIA1*	0.99 [0,64-1,56]	0.99	0.045 (0.04)	0.29	0.87 [0.62-1.21]	0.40	-0.002 (0.011)	0.84
rs2923437	8:42425399	A/C	*SMIM19, CHRNB3, SLC20A2*	0.98 [0,78-1,23]	0.88	0.047 (0.02)	**2.60E-02**	1.11 [0.94-1.31]	0.23	0.008 (0.005)	0.11
rs1922930	6:1364691	C/A	*FOXQ1, FOXF2*	0.93 [0,65-1,33]	0.70	0.035 (0.04)	0.33	NA	NA	NA	NA
rs2385089	19:18550434	A/C	*ISYNA1, ELL, LRRC25*	1.20 [0.94-1.53]	0.14	0.049 (0.03)	0.057	NA	NA	NA	NA
rs10954468	7:134434661	C/A	*BPGM, CALD1*	1.08 [0.86-1.36]	0.50	0.033 (0.02)	0.13	NA	NA	NA	NA
PVS in basal ganglia											
rs4675310 §	2:203880834	A/G	*NBEAL1, ICA1L*	1.07 [0.81-1.41]	0.61	0.01 (0.04)	0.78	1.88 [0.63-5.60]	0.26	0.046 (0.03)	0.11
rs6769442	3:171565463	G/A	*TMEM212*	1.10 [0.87-1.40]	0.37	0.03 (0.03)	0.33	1.04 [0.71-1.53]	0.82	0.008 (0.01)	0.35

PVS, perivascular spaces; EA, effective allele; OA, other allele; EAF, effective allele frequency; NA in the Nagahama Study correspond to variants that are rare (MAF<1%: rs7596872; rs1922930; rs10954468) or monomorphic (rs112407396; rs56104388) in East Asians, or not available including in EAS 1000G data (rs2385089); SNPs or tags SNPs (r^2>0.80, 1000G EAS) with a p-value<0.05 are in bold.

* The Tag SNP (r^2>0.80) is nominally significant: rs4685022 (r^2=0.81 with rs934448, 1000G EAS) p=0.048; rs4959689 (r^2=0.83 with rs1772953, 1000G EAS) p=0.02; † SNPs with a p-value < $1.09x10^{-3}$ (Bonferroni correction for 23 independent loci and two PVS locations); ‡ SNPs reaching genome-wide significance; § the lead SNP for this locus is not present in the Nagahama Study, we used a tag SNP (rs150788469, r^2=1.0 with rs4675310) where A allele of rs4675310 is in phase with G of rs150788469.

METHODS

Study design

Analyses were performed on stroke-free participants from 21 population-based cohorts (18 population-based cohorts for the GWAS meta-analysis), taking part in the Cohorts for Heart and Aging Research in Genomic Epidemiology (CHARGE) consortium, the BRrain Imaging, cognitive, Dementia, and next-generation Genomics (BRIDGET) initiative, and from the UK Biobank (UKB). Characteristics of study participants for each cohort are provided in **Supplementary Table 1-3**. All participants gave written informed consent, and institutional review boards approved individual studies (**Supplementary Table 1**).

Perivascular space burden definition

PVS were defined as fluid filled spaces with a signal identical to that of cerebral spinal fluid (CSF) of round, ovoid, or linear shape depending on the slice direction, with usually a maximum diameter smaller than 3 mm, and located in areas supplied by perforating arteries. PVS do not have a hyperintense rim on T2-weighted or FLAIR sequences.[3] In most CHARGE cohorts visual semi-quantitative rating scales were used to quantify PVS burden. As different scales were used across studies we dichotomized PVS burden into "extensive PVS burden" versus the rest in each cohort, defined by a cut-off closest to the top quartile of the semi-quantitative scale distribution (**Supplementary Methods, Supplementary Table 2)**. We chose to dichotomize PVS burden using PVS grades or numbers equal to or larger than the 75th percentile of the distribution as a cut-off. This threshold was chosen because (i) small PVS counts are very sensitive to MRI field strength and less prominently associated with age and vascular risk factors;[60] (ii) extreme burden of other MRI-markers of cSVD (e.g. extensive white

matter hyperintensity burden within the top quartile of the distribution) was previously shown to be a powerful method to facilitate the identification of genetic variants underlying cSVD.[61] We chose to compare persons in the top quartile of the PVS distribution within each cohort to other participants of that cohort rather than define a similar level of severity across cohorts, as this is highly dependent on participant characteristics, especially age, PVS quantification methods, and image acquisition parameters. In the Rotterdam Study III (RSIII) and in UKB a novel automated method was used to detect the number of PVS (**Supplementary Methods)**. We dichotomized PVS burden in RSIII and UKB using the top quartile as the cut-off. For sensitivity analyses we also compared results obtained in UKB with the dichotomized PVS variable to results obtained with the continuous measure (log-transformed to obtain a normal distribution).

Covariates and descriptive variables

Total intracranial volume was available in all studies except ASPS, and was defined as the sum of grey matter, white matter and CSF volumes. Brain parenchymal fraction was used in ASPS and defined as the ratio of brain parenchymal tissue volume to total volume within the surface contour of the whole brain. Other covariates are described in the **Supplementary Methods**.

Genotyping and imputation

Genome wide genotypes were imputed to the 1000 Genomes project (1000G) phase I v3 or the Haplotype Reference Consortium (HRC) reference panels (**Supplementary Table 3**).

PVS genome-wide association analyses in individual cohorts

Ancestry-specific logistic regression analyses with an additive genetic model were performed, adjusting for age, sex (genetically determined), and total intracranial volume (or brain parenchymal fraction for ASPS), relevant principal components of population stratification, and study site.

As a sensitivity analysis we also ran a linear regression in UKB, using the log-transformed continuous PVS measurements and adjusting for the same variables as above.

PVS genome-wide-association meta-analyses

First we performed quality control (QC) in each study following recommendations of Winkler et al.[62] Analyses were done on autosomal biallelic markers. Duplicate markers were removed, marker names and alleles were harmonized across studies, and P-Z plots (to check if the erroneous p-values are removed), quantile-quantile (QQ) plots and allele frequency-plots were constructed. In each study rare variants (minor allele frequency (MAF) < 0.01), variants with low imputation accuracy (R^2, oevar_imp or info score < 0.5) and extensive effect size values ($\beta>5$ or $\beta<-5$) were removed. The number of SNPs passing QC for each study is reported in **Supplementary Table 4**. We conducted a sample size weighted GWAS meta-analysis of all participating cohorts using METAL. This approach is most appropriate as PVS were measured on different scales in the various cohorts **(Supplementary Methods)**. First, a sample size weighted meta-analysis was conducted in each ancestry group (European (EUR), Asian (ASN), African-American (AA), Hispanics (HISP)) using METAL, followed by a meta-analysis across ancestries.[63] Genomic control was applied to each study-specific GWAS with a genomic inflation factor greater than 1.00. The effective allele count was defined as twice the product of the MAF, imputation accuracy and number of participants with extensive PVS. Variants with

an effective allele count <10 were excluded from the meta-analysis. So were variants with significant heterogeneity (Phet<5.0×10^{-8}). We performed LD clumping, sorting the genome-wide significant SNPs by p-value, keeping the most significant SNP and removing SNPs with an r^2>0.1 within 1 Mb. Only variants present in at least half of the participants of the final meta-analysis were used to construct QQ and Manhattan plots. As secondary analyses, we also ran inverse-variance weighted meta-analyses to obtain effect estimates and standard errors for follow-up bioinformatics analyses.

PVS next generation sequencing association analyses

Using whole exome sequencing (WES) and exome content of whole genome sequencing (WGS) data in 19,178 participants from UKB and the BRIDGET consortium, of whom 4,531, 4,424, and 4,497 had extensive PVS in WM, BG, and HIP respectively, we performed a whole exome association study (WEAS) to identify (rare) exonic variants associated with extensive PVS (**Supplementary Methods, Supplementary Table 1, Supplementary Results**).

Conditional and joint multiple-SNP analysis

We used Genome-wide Complex Trait Analysis (GCTA)-COJO[64] to perform conditional and joint multiple-SNP analysis of PVS GWAS summary statistics, with LD correction between SNPs, to identify secondary association signals at each of the genome-wide significant loci within 1 Mb of the lead SNP. We used European GWAS summary statistics as recommended to avoid population stratification. This method relied on a stepwise selection procedure to select SNPs based on the conditional p-values, and the joint effects of all selected SNPs after optimization of the model was estimated.[64] We used genotypes of 6,489 unrelated European participants from the 1000 Genomes imputed 3C-Dijon study data for LD correction.

Trans-ethnic meta-regression of genome-wide association studies

We conducted a multi-ancestry meta-analysis using the MR-MEGA software,[65] which uses meta-regression to model allelic effects including axes of genetic variation as covariates in the model.

Gene based analysis

We performed gene-based analyses on European PVS GWAS meta-analysis. First we used the Multi-marker Analysis of GenoMic Annotation (MAGMA) software[66] implemented in FUMA[67] to perform a gene-based association study including 19,037 protein coding genes. This method is based on a multiple linear principal components regression model. We included variants located within 10kb of the 3' and 5' UTRs of a gene to include regulatory variants. Gene-wide significance was defined at $p<2.63x10^{-6}$. We also performed gene-based tests using the VEGAS2 software,[68] including 18,371 autosomal genes, leading to a gene-wide significance at $p<2.72x10^{-6}$. We included variants located within 10kb of the 3' and 5' UTRs of a gene to capture regulatory variants. Genes were considered in the same locus if they were <200kb of each other.

PVS heritability estimates

We used LD-score regression (ldsc package https://github.com/bulik/ldsc/) to estimate the heritability of extensive PVS burden in each location.

Multitrait analysis of PVS GWAS with GWAS of other MRI-markers of cSVD

We conducted a joint analysis of summary statistics from GWAS of PVS, WMH and lacunes with a Multi-Trait Analysis of GWAS (MTAG).[69] Because of the genetic correlation between these MRI-markers of cSVD, we expected to gain in power with MTAG by incorporating information contained in the GWAS estimates for the other MRI-markers of cSVD. MTAG results are obtained after estimating the variance-covariance matrix of the GWAS estimation error using LD score regression and the variance-covariance matrix of the SNP effects using method of moments. The MTAG method is based on a generalized model and the MTAG estimator is a weighted sum of the GWAS estimates. Of all genome-wide significant risk variants for PVS burden resulting from the MTAG analysis, only variants with a p-value < 0.05 in the univariate PVS GWAS and showing greater significance in MTAG than in univariate analyses for PVS, WMH, and lacunes were prioritized.

Validation and expansion of findings across the lifespan and across ancestries

We explored association of WM and BG PVS risk variants identified in the GWAS meta-analysis with WM and BG PVS burden in a cohort of young adults (i-Share study, N=1,748, mean age 22.1±2.3 years) and in an older Japanese population-based sample (Nagahama study, N=2,862, mean age 68.3±5.3 years) to assess whether our findings also apply to these populations (**Supplementary Methods**). In each study we used both quantitative PVS measurements derived from a computational AI-based method (**Supplementary Methods**), and dichotomized PVS burden (top quartile of PVS distribution, **Supplementary Table 2**). HIP PVS were not available. Continuous PVS measurements were log-transformed to obtain a normal distribution. Association analyses were adjusted for sex, age at MRI, intracranial volume, and the first four principal components of population stratification (**Supplementary Methods**, **Supplementary Table 1 and 3**). In the Nagahama Study, when the lead SNP from

144 the PVS GWAS meta-analysis was not present, we used a tag SNP with r^2>0.80 using 1000G
145 EAS reference panel (**Supplementary Table 2**; **Supplementary Methods**). In i-Share European
146 participants we also explored the association of WM-PVS with a weighted genetic risk score
147 (wGRS) of WM-PVS burden, including the 21 independent SNPs identified in the European
148 GWAS (r^2<0.10 based on the 1000G European reference panel). SNPs were weighted by the
149 effects of the SNPs in the European ancestry GWAS meta-analysis, the effect allele being the
150 allele associated with increased PVS burden; the wGRS was rescaled (rwGRS) so that one unit
151 of the genetic risk score corresponds to one additional WM-PVS risk allele. We tested for a
152 significant modifying effect of age on associations with WM-PVS for the three genome-wide
153 significant WM-PVS loci that also showed significant associations with extensive WM-PVS in
154 young adults. For this purpose we collected the effect estimates (along with their standard
155 errors) for the lead SNPs at these three loci in each individual cohort. We fitted a meta-
156 regression of the lead SNPs' effect sizes onto an intercept and age. Meta-regression analysis
157 was performed using the Metafor package in R, and any statistical evidence of linear
158 association was corrected for multiple testing (Bonferroni correction), using $p<0.05/3=1.7x10^{-2}$
159 (**Supplementary Methods**).
160
161 **Shared genetic variation with other phenotypes**
162 To explore shared genetic variation with vascular and neurological phenotypes, analyses were
163 conducted on the European ancestry meta-analysis. These phenotypes included: (i) putative
164 risk factors (SBP, DBP, pulse pressure (PP), body mass index (BMI), high density lipoprotein
165 (HDL) cholesterol, low density lipoprotein (LDL) cholesterol, triglycerides, type 2 diabetes, and
166 sleep patterns); (ii) other MRI-markers of brain aging (WMH burden, covert MRI-defined brain
167 infarcts and lacunes, and hippocampal, accumbens, amygdala, caudate, pallidum and

putamen volumes); and (iii) the most common neurological conditions previously reported to be associated with PVS, namely stroke (any stroke, any ischemic stroke, large artery stroke, cardio-embolic stroke, small vessel stroke, intracerebral hemorrhage [ICH]), AD, and Parkinson disease (**Supplementary Methods**). Summary statistics of the largest publicly available GWAS were obtained.

First, we explored whether genome-wide significant PVS risk loci (lead variants or variants in linkage disequilibrium with $r^2>0.9$, based on the 1000G European reference panel) were associated with these traits. A p-value threshold $<3.3x10^{-5}$ correcting for 21 independent phenotypes, for the 3 PVS locations and for the 24 independent loci tested was used (**Supplementary Methods**). We performed a colocalization analysis using the R package COLOC to search for evidence for a single causal variant between PVS and the other phenotypes. A large posterior probability PP4 (>75%) supports a single causal variant common to both traits.[70]

Second, we used LD-score regression (ldsc package https://github.com/bulik/ldsc/) to estimate the genetic correlation of extensive PVS burden with these phenotypes ($p<7.9x10^{-4}$ was used as a significance threshold correcting for 21 phenotypes and 3 PVS locations). To decrease the potential bias due to poor imputation quality, the summary statistics were filtered to the subset of HapMap 3 SNPs for each trait.

We used the Functional Mapping and Annotation of Genome-Wide Association Studies (FUMA GWAS) platform to obtain extensive functional annotation for genome-wide significant SNPs.[67] We identified, among the genome-wide significant risk variants for extensive PVS, SNPs that were associated with another trait from the GWAS catalog at genome-wide significance **(Supplementary Methods)**.

Mendelian randomization

We used a Mendelian randomization approach to explore the causal relation of putative risk factors (SBP, DBP, PP, BMI, LDL- and HDL-cholesterol, triglycerides, type 2 diabetes, and sleep patterns) with extensive PVS burden, and of extensive PVS burden with neurological traits (stroke, AD and Parkinson diseases).

First, we used the Generalised Summary-data-based Mendelian Randomisation (GSMR) method implemented in the GCTA software.[71] The summary statistics were clumped using the 1000G imputed 3C-Dijon study data (r^2<0.05 and p<$5x10^{-8}$), and only SNPs with a MAF >0.01 were used. The heterogeneity in independent instrument (HEIDI)-outlier method was used to remove genetic instruments that showed pleiotropic effects on both the exposure and the outcome.

For nominally significant GSMR associations we conducted secondary MR analyses using both TwoSampleMR and RadialMR.[72,73] In both analyses, only independent SNPs (r^2<0.01 based on 1000 Genomes European sample, window size = 1 Mb) reaching genome-wide significance (p<$5x10^{-8}$) in the primary meta-analysis were included as recommended (**Supplementary Methods**). Effect estimates (betas) and standard errors (SEs) used for SNP weights were derived from the inverse-variance weighted GWAS meta-analyses. With TwoSampleMR, we estimated the effect of each exposure on each outcome using weighted median, random-effect inverse-variance weighting (IVW) and MR-Egger. In addition, we confirmed the directionality of the observed associations with the Steiger test (**Supplementary Methods**). With RadialMR, the putative causal effect of each exposure on each outcome was estimated using the fixed-effect IVW method using the modified-second order inverse variance weight (**Supplementary Methods**).[73] Cochran's Q statistic was used to test for the presence of heterogeneity (p<0.05) due to horizontal pleiotropy that occurs when instruments affect the

outcome independently of the exposure.[73] Outlier SNPs were identified by regressing the predicted causal estimate against the inverse variance weights.[73] After excluding these SNPs, we re-ran IVW tests, as well as MR-Egger regression, assessing heterogeneity using Rücker's Q' statistic.[73] We calculated the Q_R statistic as the ratio of Q' (Egger) on Q (IVW). A Q_R close to 1 indicates that both IVW and MR-Egger models fit the data equally well and made us select the IVW model. We formally ruled out horizontal pleiotropy when the results for models showed a non-significant ($p \geq 0.05$) MR-Egger intercept after exclusion of outliers. To account for potential residual correlated pleiotropy we used MR-CAUSE.[74] Finally, we explored the association between genetic liability to BG PVS and stroke conditioning on blood pressure (diastolic and systolic blood pressure separately) by running multivariable MR analyses using TwoSampleMR.[72] A $p<1.19 \times 10^{-3}$ correcting for 14 independent phenotypes and the 3 PVS locations was considered significant.

Pathway analyses

We conducted pathway analyses on European PVS summary statistics, and used the 1000G phase 3 reference panel. We used MAGMA gene set analyses **(Supplementary Methods)** implemented in FUMA[67] to identify pathways overrepresented in the associations. We identified genes associated with extensive PVS burden and estimated the correlation between genes, reflecting the LD between genes. The p-values and gene correlation matrix were used in a generalized least squares model. A p-value $<3.2 \times 10^{-6}$ correction for 15,496 gene sets was considered significant. As a sensitivity analysis, we used the VEGAS2Pathway approach,[75] which aggregates association strengths of individual markers into pre-specified biological pathways using VEGAS-derived gene association p-values for extensive PVS burden. The

empirical significance threshold for VEGAS2Pathway was $1x10^{-5}$ accounting for 6,213 correlated pathways.

Enrichment analyses in OMIM and COSMIC genes

Using a hypergeometric test we performed enrichment analyses of genes within 1 Mb, 100 kb or 10 kb of the lead variants, but also of genes within 10 kb of the lead variants with intragenic variants, and genes within 10 kb of the genetic loci with intragenic lead variants. We used the rest of the protein-coding genome as reference. We performed the analysis first combining the loci of the 3 PVS locations, and second including only WM PVS burden loci. We searched for an enrichment in different genes groups from the Online Mendelian Inheritance in Man (OMIM) database,[76] including perivascular spaces (*"perivascular space" OR "virchow-robin space"*), white matter hyperintensities (*leukoaraiosis OR "white matter lesion" OR "white matter hyperintensities"*) and leukodystrophy (*leukodystrophy OR leukoencephalopathy*) genes. We also searched for an enrichment of genes involved in glioma and glioblastoma identified in the catalogue of somatic mutations in cancer (COSMIC, https://cancer.sanger.ac.uk).

Transcriptome-wide association study

We performed transcriptome-wide association studies (TWAS) using TWAS-Fusion[77] to identify genes whose expression is significantly associated with PVS burden without directly measuring expression levels. We restricted the analysis to tissues considered relevant for cerebrovascular disease, and used precomputed functional weights from 22 publicly available gene expression reference panels from blood, arterial, brain and peripheral nerve tissues (**Supplementary Methods**). TWAS-Fusion was then used to estimate the TWAS association

statistics between predicted gene expression and PVS burden by integrating information from expression reference panels (SNP-expression weights), GWAS summary statistics (SNP-PVS effect estimates), and LD reference panels (SNP correlation matrix). Transcriptome-wide significant genes (eGenes) and the corresponding QTLs (eQTLs) were determined using Bonferroni correction (p-value $<3.93 \times 10^{-6}$, **Supplementary Methods**). eGenes were then tested in conditional analysis as implemented in TWAS-Fusion. Next we performed a genetic colocalization analysis of gene expression and PVS burden for each conditionally significant gene ($p<0.05$) using the COLOC R package,[70] in order to estimate the posterior probability of a shared causal variant (posterior probability PP4 ≥0.75) between the gene expression and the trait. Gene regions with eQTLs not reaching genome-wide significance in association with PVS, and not in LD ($r^2<0.01$) with the lead SNP for genome-wide significant PVS risk loci, were considered as novel**.**

Cell type enrichment analysis

We conducted a cell-type enrichment analysis using **S**ingle cell **T**ype **E**nrichment **A**nalysis for **P**henotypes (https://github.com/erwinerdem/STEAP/). This is an extension to CELLECT and uses S-LDSC, MAGMA, and H-MAGMA for enrichment analysis **(Supplementary Methods)**. PVS GWAS summary statistics were first munged. Then, expression specificity profiles were calculated using human and mouse single cell RNA-seq databases (**Supplementary Table 24**). Cell-type enrichment was calculated with three models : MAGMA, H-MAGMA (incorporating chromatin interaction profiles from human brain tissues in MAGMA) and stratified LD score regression. P-values were corrected for the number of independent cell-types in each database (Bonferroni correction).

Enrichment in drug target genes

We used the GREP (Genome for Repositioning)[78] software tool that quantifies an enrichment of gene sets from GWAS summary statistics in drugs of certain ATC classes or indicated for some ICD10 disease categories and captures potentially repositionable drugs targeting the gene set. Genes significantly detected (FDR-q <0.1) in MAGMA software were used for enrichment analyses in GREP software with the target genes of approved or investigated drugs curated in DrugBank and Therapeutic Target Database.

We used the Trans-Phar (integration of TWAS and Pharmacological database) software to identify drug target candidates in a specific tissue or cell-type category.[79] First a TWAS using FOCUS, which demonstrates fine-mapping of causal gene sets from TWAS results, and 27 tissues in GTEx v7 database (corresponding to defined 13 tissue-cell-type categories assigned by the 27 tissues in GTEx v7 database and 77 LINCS CMap L1000 library cell types) was performed to identify up- and down-regulated genes in participants with extensive PVS burden, and select the top 10% genes with the highest expression variation. Then we performed a negative Spearman's rank correlation analysis between the top 10% genes expression (Z-score) and the LINCS CMap L1000 library database.

Lifetime brain gene expression profile

We studied the lifetime expression of the genes identified in the TWAS and GWAS analyses, and the 3 genes associated with WM PVS burden in both the old and young populations to search for developmental processes. We used a public database https://hbatlas.org/ comprising genome-wide exon-level transcriptome data from 1,340 tissue samples from 16 brain regions (cerebellar cortex, mediodorsal nucleus of the thalamus, striatum, amygdala, hippocampus, and 11 areas of the neocortex) of 57 postmortem human brains, from

311 embryonic development to late adulthood men and women of different ancestries
312 (**Supplementary Methods**).
313
314
315 **REFERENCES**
316
317 **ACKNOWLEDGEMENTS**
318 Detailed acknowledgements are included in the **Supplementary Appendix.** We thank all the
319 participating cohorts for contributing to this study. We thank Dr. Hélène Jacqmin-Gadda,
320 Bordeaux Population Health research center, University of Bordeaux / Inserm U1219 for
321 statistical advice. We thank Dr. Judith Thomas-Crusells for editorial assistance.
322
323 **AUTHOR CONTRIBUTIONS**
324 F.M., C.T., J.M.W., S.Seshadri, H.H.H.A., and S.D. jointly supervised research. M-G.D., M.J.K.,
325 Q.LG., T.E.E., A.M., and A.Tsuchida contributed equally. M-G.D., M.J.K., H.H.H.A. and S.D.
326 designed and conceived the study. J.R.R., S.F., M.L., E.H., M.B., N.D.D., P.D., S.H., R.M.T., F.D.,
327 J.S., Y.S., N.J.A., C.B., M.E.B., A.B., H.B., R.B., C.C., C.Chen, C-Y.C, I.J.D., P.G.G., J.J.H., J.J., T.K.,
328 S. L., M.M., P.M., Z.M., S.M-M., S.M., M.O., M.P., P.P., T.R., M.S., S.S., K.S., O.S., Y.T., A.T.,
329 A.Thalamuthu, J.N.T., M.C.V-H, M.W.V., U.V., K.W., T.Y.W., M.J.W., Q.Y., J.Z., W.Z., Y.Z., H.S.,
330 P.S.S., W.W., K.Y.,C.L.S., R.L.S., G.B., M.Lathrop., I.F-C., B.M., P.B., H.J.G., K.A.M., R.S., M.J., and
331 M.A.I. generated the PVS phenotype, genomic data and conducted cohort-wise GWAS
332 analyses. G.R., T.K., D-A.T., A.J.,T.P. and Y.O. contributed to bioinformatics analyses. M-G.D.
333 and S.D., M.J.K., Q.LG., T.E.E., A.M., A.Tsuchida, F. M., C.T., J.M.W., S.Seshadri, and H.H.A.
334 wrote and edited the manuscript.

DATA AVAILABILITY

Genome-wide summary statistics for the European and combined meta-analysis generated and analyzed during the current study are deposited on the CHARGE Consortium Summary Results from Genomic Studies repository on dbGaP (accession number phs000930.v10.p1). The PVS quantification method used in the Nagahama Study is available using this link: https://github.com/pboutinaud/SHIVA_PVS. All other data supporting the findings of this study are available either within the article, the supplementary information and supplementary data files, or from the authors upon reasonable request.

COMPETING INTERESTS

The authors declared no potential conflicts of interest with respect to research, authorship, and/or publication of this article.

1. Pollock, H., Hutchings, M., Weller, R.O. & Zhang, E.T. Perivascular spaces in the basal ganglia of the human brain: their relationship to lacunes. *J Anat* **191 (Pt 3)**, 337-346 (1997).
2. Wardlaw, J.M.*, et al.* Perivascular spaces in the brain: anatomy, physiology and pathology. *Nat Rev Neurol* **16**, 137-153 (2020).
3. Wardlaw, J.M.*, et al.* Neuroimaging standards for research into small vessel disease and its contribution to ageing and neurodegeneration. *The Lancet Neurology* **12**, 822-838 (2013).
4. Jessen, N.A., Munk, A.S.F., Lundgaard, I. & Nedergaard, M. The Glymphatic System: A Beginner's Guide. *Neurochemical Research* **40**, 2583-2599 (2015).
5. Yao, M.*, et al.* Hippocampal perivascular spaces are related to aging and blood pressure but not to cognition. *Neurobiology of Aging* **35**, 2118-2125 (2014).
6. Sargurupremraj, M.*, et al.* Cerebral small vessel disease genomics and its implications across the lifespan. *Nat Commun* **11**, 6285 (2020).
7. Debette, S., Schilling, S., Duperron, M.G., Larsson, S.C. & Markus, H.S. Clinical Significance of Magnetic Resonance Imaging Markers of Vascular Brain Injury: A Systematic Review and Meta-analysis. *JAMA Neurol* **76**, 81-94 (2019).
8. Mestre, H., Kostrikov, S., Mehta, R.I. & Nedergaard, M. Perivascular spaces, glymphatic dysfunction, and small vessel disease. *Clin Sci (Lond)* **131**, 2257-2274 (2017).

9. Deramecourt, V.*, et al.* Staging and natural history of cerebrovascular pathology in dementia. *Neurology* **78**, 1043-1050 (2012).
10. Bacyinski, A., Xu, M., Wang, W. & Hu, J. The Paravascular Pathway for Brain Waste Clearance: Current Understanding, Significance and Controversy. *Front Neuroanat* **11**, 101 (2017).
11. Duperron, M.G.*, et al.* High dilated perivascular space burden: a new MRI marker for risk of intracerebral hemorrhage. *Neurobiol Aging* **84**, 158-165 (2019).
12. Charidimou, A.*, et al.* MRI-visible perivascular spaces in cerebral amyloid angiopathy and hypertensive arteriopathy. *Neurology* **88**, 1157-1164 (2017).
13. Tsai, H.H.*, et al.* Centrum Semiovale Perivascular Space and Amyloid Deposition in Spontaneous Intracerebral Hemorrhage. *Stroke* **52**, 2356-2362 (2021).
14. Charidimou, A. & al., e. Abstract 36: The Boston Criteria V2.0 for Cerebral Amyloid Angiopathy: Updated Criteria and Multicenter MRI-Neuropathology Validation. *Stroke* **52:A36**(2021).
15. Mestre, H.*, et al.* Cerebrospinal fluid influx drives acute ischemic tissue swelling. *Science* **367**(2020).
16. Månberg, A.*, et al.* Altered perivascular fibroblast activity precedes ALS disease onset. *Nat Med* **27**, 640-646 (2021).
17. Duperron, M.G.*, et al.* Burden of Dilated Perivascular Spaces, an Emerging Marker of Cerebral Small Vessel Disease, Is Highly Heritable. *Stroke* (2018).
18. Bouvy, W.H.*, et al.* Visualization of perivascular spaces and perforating arteries with 7 T magnetic resonance imaging. *Investigative radiology* **49**, 307-313 (2014).
19. Psaty, B.M.*, et al.* Cohorts for Heart and Aging Research in Genomic Epidemiology (CHARGE) Consortium: Design of prospective meta-analyses of genome-wide association studies from 5 cohorts. *Circ Cardiovasc Genet* **2**, 73-80 (2009).
20. Bordes, C., Sargurupremraj, M., Mishra, A. & Debette, S. Genetics of common cerebral small vessel disease. *Nat Rev Neurol* **18**, 84-101 (2022).
21. Joutel, A., Haddad, I., Ratelade, J. & Nelson, M.T. Perturbations of the cerebrovascular matrisome: A convergent mechanism in small vessel disease of the brain? *J Cereb Blood Flow Metab* **36**, 143-157 (2016).
22. Traylor, M.*, et al.* Genetic basis of lacunar stroke: a pooled analysis of individual patient data and genome-wide association studies. *The Lancet. Neurology* (2021).
23. Persyn, E.*, et al.* Genome-wide association study of MRI markers of cerebral small vessel disease in 42,310 participants. *Nat Commun* **11**, 2175 (2020).
24. Simon, A.J.*, et al.* Mutations in STN1 cause Coats plus syndrome and are associated with genomic and telomere defects. *The Journal of experimental medicine* **213**, 1429-1440 (2016).
25. Whittaker, E.*, et al.* Systematic Review of Cerebral Phenotypes Associated With Monogenic Cerebral Small-Vessel Disease. *J Am Heart Assoc* **11**, e025629 (2022).
26. Piantino, J.*, et al.* Characterization of MR Imaging-Visible Perivascular Spaces in the White Matter of Healthy Adolescents at 3T. *AJNR Am J Neuroradiol* **41**, 2139-2145 (2020).
27. Rajani, R.M.*, et al.* Reversal of endothelial dysfunction reduces white matter vulnerability in cerebral small vessel disease in rats. *Science Translational Medicine* **10**, eaam9507 (2018).
28. Carelli, V.*, et al.* Syndromic parkinsonism and dementia associated with OPA1 missense mutations. *Ann Neurol* **78**, 21-38 (2015).
29. Herkenne, S.*, et al.* Developmental and Tumor Angiogenesis Requires the Mitochondria-Shaping Protein Opa1. *Cell Metab* **31**, 987-1003.e1008 (2020).
30. Backhouse, E.V.*, et al.* Early life predictors of late life cerebral small vessel disease in four prospective cohort studies. *Brain : a journal of neurology* **144**, 3769-3778 (2021).
31. Zhao, B.*, et al.* Common genetic variation influencing human white matter microstructure. *Science* **372**(2021).
32. Grasby, K.L.*, et al.* The genetic architecture of the human cerebral cortex. *Science* **367**(2020).
33. Mok, V.*, et al.* Race-ethnicity and cerebral small vessel disease – Comparison between Chinese and White populations. *International Journal of Stroke* **9**, 36-42 (2014).

34. Akinyemi, R.O*., et al.* Stroke, cerebrovascular diseases and vascular cognitive impairment in Africa. *Brain research bulletin* **145**, 97-108 (2019).
35. Mollink, J*., et al.* The spatial correspondence and genetic influence of interhemispheric connectivity with white matter microstructure. *Nat Neurosci* **22**, 809-819 (2019).
36. Gaire, B.P., Sapkota, A., Song, M.R. & Choi, J.W. Lysophosphatidic acid receptor 1 (LPA1) plays critical roles in microglial activation and brain damage after transient focal cerebral ischemia. *J Neuroinflammation* **16**, 170 (2019).
37. Gross, I. & Brauer, A.U. Modulation of lysophosphatidic acid (LPA) receptor activity: the key to successful neural regeneration? *Neural Regen Res* **15**, 53-54 (2020).
38. Hisaoka-Nakashima, K*., et al.* Mirtazapine increases glial cell line-derived neurotrophic factor production through lysophosphatidic acid 1 receptor-mediated extracellular signal-regulated kinase signaling in astrocytes. *Eur J Pharmacol* **860**, 172539 (2019).
39. Allanore, Y*., et al.* Lysophosphatidic Acid Receptor 1 Antagonist SAR100842 for Patients With Diffuse Cutaneous Systemic Sclerosis: A Double-Blind, Randomized, Eight-Week Placebo-Controlled Study Followed by a Sixteen-Week Open-Label Extension Study. *Arthritis Rheumatol* **70**, 1634-1643 (2018).
40. Stenman, J.M*., et al.* Canonical Wnt signaling regulates organ-specific assembly and differentiation of CNS vasculature. *Science* **322**, 1247-1250 (2008).
41. Chavali, M*., et al.* Wnt-Dependent Oligodendroglial-Endothelial Interactions Regulate White Matter Vascularization and Attenuate Injury. *Neuron* **108**, 1130-1145.e1135 (2020).
42. Capone, C*., et al.* Reducing Timp3 or vitronectin ameliorates disease manifestations in CADASIL mice. *Ann Neurol* **79**, 387-403 (2016).
43. Tanaka, T*., et al.* Plasma proteomic signatures predict dementia and cognitive impairment. *Alzheimers Dement (N Y)* **6**, e12018 (2020).
44. Jakobsson, L., Domogatskaya, A., Tryggvason, K., Edgar, D. & Claesson-Welsh, L. Laminin deposition is dispensable for vasculogenesis but regulates blood vessel diameter independent of flow. *Faseb j* **22**, 1530-1539 (2008).
45. Yao, Y., Chen, Z.L., Norris, E.H. & Strickland, S. Astrocytic laminin regulates pericyte differentiation and maintains blood brain barrier integrity. *Nat Commun* **5**, 3413 (2014).
46. Chung, J*., et al.* Genome-wide association study of cerebral small vessel disease reveals established and novel loci. *Brain : a journal of neurology* **142**, 3176-3189 (2019).
47. Armstrong, N.J*., et al.* Common Genetic Variation Indicates Separate Causes for Periventricular and Deep White Matter Hyperintensities. *Stroke* **51**, 2111-2121 (2020).
48. Hadano, S*., et al.* A gene encoding a putative GTPase regulator is mutated in familial amyotrophic lateral sclerosis 2. *Nat Genet* **29**, 166-173 (2001).
49. Bindesbøll, C*., et al.* NBEAL1 controls SREBP2 processing and cholesterol metabolism and is a susceptibility locus for coronary artery disease. *Sci Rep* **10**, 4528 (2020).
50. Wang, W.W., Gallo, L., Jadhav, A., Hawkins, R. & Parker, C.G. The Druggability of Solute Carriers. *J Med Chem* **63**, 3834-3867 (2020).
51. Dewulf, J.P*., et al.* SLC13A3 variants cause acute reversible leukoencephalopathy and α-ketoglutarate accumulation. *Ann Neurol* **85**, 385-395 (2019).
52. Beyens, A*., et al.* Arterial tortuosity syndrome: 40 new families and literature review. *Genet Med* **20**, 1236-1245 (2018).
53. Wang, C*., et al.* Mutations in SLC20A2 link familial idiopathic basal ganglia calcification with phosphate homeostasis. *Nat Genet* **44**, 254-256 (2012).
54. Ho, H.T., Dahlin, A. & Wang, J. Expression Profiling of Solute Carrier Gene Families at the Blood-CSF Barrier. *Front Pharmacol* **3**, 154 (2012).
55. Wang, H*., et al.* Structure, function, and genomic organization of human Na(+)-dependent high-affinity dicarboxylate transporter. *Am J Physiol Cell Physiol* **278**, C1019-1030 (2000).
56. Mestre, H*., et al.* Flow of cerebrospinal fluid is driven by arterial pulsations and is reduced in hypertension. *Nat Commun* **9**, 4878 (2018).

57. Wardlaw, J.M.*, et al.* Neuroimaging standards for research into small vessel disease and its contribution to ageing and neurodegeneration. *Lancet Neurol* **12**, 822-838 (2013).
58. Rannikmäe, K.*, et al.* COL4A2 is associated with lacunar ischemic stroke and deep ICH: Meta-analyses among 21,500 cases and 40,600 controls. *Neurology* **89**, 1829-1839 (2017).
59. Ballerini, L.*, et al.* Computational quantification of brain perivascular space morphologies: Associations with vascular risk factors and white matter hyperintensities. A study in the Lothian Birth Cohort 1936. *NeuroImage. Clinical* **25**, 102120 (2020).
60. Bouvy, W.H.*, et al.* Perivascular spaces on 7 Tesla brain MRI are related to markers of small vessel disease but not to age or cardiovascular risk factors. *Journal of Cerebral Blood Flow & Metabolism* **36**, 1708-1717 (2016).
61. Mishra, A.*, et al.* Gene-mapping study of extremes of cerebral small vessel disease reveals TRIM47 as a strong candidate. *Brain : a journal of neurology* (2022).
62. Winkler, T.W.*, et al.* Quality control and conduct of genome-wide association meta-analyses. *Nat Protoc* **9**, 1192-1212 (2014).
63. Willer, C.J., Li, Y. & Abecasis, G.R. METAL: fast and efficient meta-analysis of genomewide association scans. *Bioinformatics* **26**, 2190-2191 (2010).
64. Yang, J.*, et al.* Conditional and joint multiple-SNP analysis of GWAS summary statistics identifies additional variants influencing complex traits. *Nat Genet* **44**, 369-375, S361-363 (2012).
65. Magi, R.*, et al.* Trans-ethnic meta-regression of genome-wide association studies accounting for ancestry increases power for discovery and improves fine-mapping resolution. *Hum Mol Genet* **26**, 3639-3650 (2017).
66. de Leeuw, C.A., Mooij, J.M., Heskes, T. & Posthuma, D. MAGMA: generalized gene-set analysis of GWAS data. *PLoS Comput Biol* **11**, e1004219 (2015).
67. Watanabe, K., Taskesen, E., van Bochoven, A. & Posthuma, D. Functional mapping and annotation of genetic associations with FUMA. *Nat Commun* **8**, 1826 (2017).
68. Mishra, A. & Macgregor, S. VEGAS2: Software for More Flexible Gene-Based Testing. *Twin Res Hum Genet* **18**, 86-91 (2015).
69. Turley, P.*, et al.* Multi-trait analysis of genome-wide association summary statistics using MTAG. *Nat Genet* **50**, 229-237 (2018).
70. Giambartolomei, C.*, et al.* Bayesian test for colocalisation between pairs of genetic association studies using summary statistics. *PLoS Genet* **10**, e1004383 (2014).
71. Zhu, Z.*, et al.* Causal associations between risk factors and common diseases inferred from GWAS summary data. *Nat Commun* **9**, 224 (2018).
72. Hemani, G.*, et al.* The MR-Base platform supports systematic causal inference across the human phenome. *eLife* **7**(2018).
73. Bowden, J.*, et al.* Improving the visualization, interpretation and analysis of two-sample summary data Mendelian randomization via the Radial plot and Radial regression. *Int J Epidemiol* **47**, 1264-1278 (2018).
74. Morrison, J., Knoblauch, N., Marcus, J.H., Stephens, M. & He, X. Mendelian randomization accounting for correlated and uncorrelated pleiotropic effects using genome-wide summary statistics. *Nat Genet* **52**, 740-747 (2020).
75. Mishra, A. & MacGregor, S. A Novel Approach for Pathway Analysis of GWAS Data Highlights Role of BMP Signaling and Muscle Cell Differentiation in Colorectal Cancer Susceptibility. *Twin Res Hum Genet* **20**, 1-9 (2017).
76. Amberger, J.S., Bocchini, C.A., Schiettecatte, F., Scott, A.F. & Hamosh, A. OMIM.org: Online Mendelian Inheritance in Man (OMIM(R)), an online catalog of human genes and genetic disorders. *Nucleic Acids Res* **43**, D789-798 (2015).
77. Gusev, A.*, et al.* Integrative approaches for large-scale transcriptome-wide association studies. *Nat Genet* **48**, 245-252 (2016).
78. Sakaue, S. & Okada, Y. GREP: genome for REPositioning drugs. *Bioinformatics* **35**, 3821-3823 (2019).

79. Konuma, T., Ogawa, K. & Okada, Y. Integration of genetically regulated gene expression and pharmacological library provides therapeutic drug candidates. *Hum Mol Genet* **30**, 294-304 (2021).